

HEMODYNAMIC VORTEX ANALYSIS AS A MEANS OF INTRACRANIAL  
ANEURYSM RUPTURE PREDICTION

By

Kevin William Sunderland

A DISSERTATION

Submitted in partial fulfillment of the requirements for the degree of

DOCTOR OF PHILOSOPHY

In Biomedical Engineering

MICHIGAN TECHNOLOGICAL UNIVERSITY

2019

© 2019 Kevin William Sunderland



This dissertation has been approved in partial fulfillment of the requirements for the Degree of DOCTOR OF PHILOSOPHY in Biomedical Engineering.

Department of Biomedical Engineering

Dissertation Advisor: *Dr. Jingfeng Jiang*

Committee Member: *Dr. Sean Kirkpatrick #1*

Committee Member: *Dr. Gowtham #2*

Committee Member: *Dr. Min Wang #3*

Department Chair: *Dr. Sean Kirkpatrick*



## Dedication

To my famliy and friends

who



# Contents

List of Figures . . . . .	xi
List of Tables . . . . .	xiii
Preface . . . . .	xv
Acknowledgments . . . . .	xix
Definitions . . . . .	xxi
List of Abbreviations . . . . .	xxv
Abstract . . . . .	xxix
<b>1 Introduction . . . . .</b>	<b>1</b>
1.0.1 Morphological Characteristics . . . . .	3
1.0.2 Hemodynamic Characteristics . . . . .	4
1.1 Section 1 . . . . .	8
1.1.1 Objective . . . . .	8
1.1.2 Methodolgy . . . . .	9

1.2	Aneurysm Geometric Characterisitics . . . . .	10
1.3	Aneurysm Hemodynamic Characterisitics . . . . .	13
1.4	Disturbed Flow on Vascular Endothelium . . . . .	14
<b>2</b>	<b>Hemodynamic Flow Vortex Identification . . . . .</b>	<b>19</b>
2.1	Materials and Methods . . . . .	22
2.1.1	Modeling of "Patient-specific" Vasculature . . . . .	22
2.1.2	Mesh Generation . . . . .	23
2.1.3	CFD Simulation . . . . .	23
2.1.4	Aneurysm Extraction and Voxelization of Aneurismal Velocity Data . . . . .	25
2.1.5	Vortex Core Extraction and Analysis . . . . .	25
<b>3</b>	<b>Vortex Analysis to predict IA Initiation . . . . .</b>	<b>33</b>
	<b>References . . . . .</b>	<b>45</b>
<b>A</b>	<b>Statistics . . . . .</b>	<b>79</b>
A.1	Section 1 . . . . .	80
A.2	Section 2 . . . . .	84
A.3	Section 3 . . . . .	87
A.4	Section 4 . . . . .	88
A.5	Section 5 . . . . .	90



<b>B Sample Code . . . . .</b>	<b>93</b>
B.1 HelloWorld.c . . . . .	95
<b>C Letters of Permission . . . . .</b>	<b>97</b>
<b>D Cellular Biology . . . . .</b>	<b>99</b>
D.1 TUNEL-assay . . . . .	99
D.2 VCAM-1 . . . . .	100



# List of Figures

1.1	Zhou 2016 Meta-analysis of the reported low WSS rate of rupture aneurysms and the Odds Ratio for low WSS in predictive modeling	5
1.2	Schematic representation of our universe . . . . .	9
1.3	Mathematical functions plotted using TikZ package . . . . .	10
1.4	Schematic representation of a water molecule . . . . .	16
2.1	Histogram of nearest neighbors . . . . .	28
	(a) Generic . . . . .	28
	(b) 200 bins . . . . .	28
2.2	Fancy mathematical plots using TikZ package . . . . .	31
2.3	Incidence, transmission and reflection . . . . .	31
3.1	Distribution of random numbers . . . . .	38
3.2	Fibre optics . . . . .	40
3.3	A landscape view of a Turboprop engine - these are jet engine deriva- tives, still gas turbines, that extract work from the hot-exhaust jet to turn a rotating shaft, which is then used to produce thrust by some other means . . . . .	42

B.1 Two examples illustrating the relationship between the angular histogram and NE: (a) a simple laminar flow case and (b) a rotational flow (eddy) case. In both cases, the right and left plots are the vector flow field and the histogram of angular vector direction, respectively. Vector fields were decimated by a factor of 3 for better visualization. 94

# List of Tables

2.1	A portrait table: first column represents the year in which the Nobel prize in physics was awarded; second column indicates the name of the scientist and the third column is the work for which the Nobel prize was awarded . . . . .	30
3.1	Measured data points representing the relationship between $x$ and $y$	38
3.2	A landscape table: first column represents the year in which the Nobel prize in physics was awarded; second column indicates the name of the scientist and the third column is an <i>as is</i> Nobel citation . . . . .	39



# Preface

Lorem ipsum dolor sit amet, consectetur adipisicing elit, sed do eiusmod tempor incididunt ut labore et dolore magna aliqua. Ut enim ad minim veniam, quis nostrud exercitation ullamco laboris nisi ut aliquip ex ea commodo consequat. Duis aute irure dolor in reprehenderit in voluptate velit esse cillum dolore eu fugiat nulla pariatur. Excepteur sint occaecat cupidatat non proident, sunt in culpa qui officia deserunt mollit anim id est laborum.

Sed ut perspiciatis unde omnis iste natus error sit voluptatem accusantium doloremque laudantium, totam rem aperiam, eaque ipsa quae ab illo inventore veritatis et quasi architecto beatae vitae dicta sunt explicabo. Nemo enim ipsam voluptatem quia voluptas sit aspernatur aut odit aut fugit, sed quia consequuntur magni dolores eos qui ratione voluptatem sequi nesciunt.

Lorem ipsum dolor sit amet, consectetur adipisicing elit, sed do eiusmod tempor incididunt ut labore et dolore magna aliqua. Ut enim ad minim veniam, quis nostrud exercitation ullamco laboris nisi ut aliquip ex ea commodo consequat. Duis aute irure dolor in reprehenderit in voluptate velit esse cillum dolore eu fugiat nulla pariatur. Excepteur sint occaecat cupidatat non proident, sunt in culpa qui officia deserunt mollit anim id est laborum.

Sed ut perspiciatis unde omnis iste natus error sit voluptatem accusantium doloremque laudantium, totam rem aperiam, eaque ipsa quae ab illo inventore veritatis et quasi architecto beatae vitae dicta sunt explicabo. Nemo enim ipsam voluptatem quia voluptas sit aspernatur aut odit aut fugit, sed quia consequuntur magni dolores eos qui ratione voluptatem sequi nesciunt.

Lorem ipsum dolor sit amet, consectetur adipisicing elit, sed do eiusmod tempor incididunt ut labore et dolore magna aliqua. Ut enim ad minim veniam, quis nostrud exercitation ullamco laboris nisi ut aliquip ex ea commodo consequat. Duis aute irure dolor in reprehenderit in voluptate velit esse cillum dolore eu fugiat nulla pariatur. Excepteur sint occaecat cupidatat non proident, sunt in culpa qui officia deserunt mollit anim id est laborum.

Sed ut perspiciatis unde omnis iste natus error sit voluptatem accusantium doloremque laudantium, totam rem aperiam, eaque ipsa quae ab illo inventore veritatis et quasi architecto beatae vitae dicta sunt explicabo. Nemo enim ipsam voluptatem quia voluptas sit aspernatur aut odit aut fugit, sed quia consequuntur magni dolores eos qui ratione voluptatem sequi nesciunt.

Lorem ipsum dolor sit amet, consectetur adipisicing elit, sed do eiusmod tempor incididunt ut labore et dolore magna aliqua. Ut enim ad minim veniam, quis nostrud exercitation ullamco laboris nisi ut aliquip ex ea commodo consequat. Duis aute irure dolor in reprehenderit in voluptate velit esse cillum dolore eu fugiat nulla pariatur.



Excepteur sint occaecat cupidatat non proident, sunt in culpa qui officia deserunt mollit anim id est laborum.

Sed ut perspiciatis unde omnis iste natus error sit voluptatem accusantium doloremque laudantium, totam rem aperiam, eaque ipsa quae ab illo inventore veritatis et quasi architecto beatae vitae dicta sunt explicabo. Nemo enim ipsam voluptatem quia voluptas sit aspernatur aut odit aut fugit, sed quia consequuntur magni dolores eos qui ratione voluptatem sequi nesciunt.

Lorem ipsum dolor sit amet, consectetur adipisicing elit, sed do eiusmod tempor incididunt ut labore et dolore magna aliqua. Ut enim ad minim veniam, quis nostrud exercitation ullamco laboris nisi ut aliquip ex ea commodo consequat. Duis aute irure dolor in reprehenderit in voluptate velit esse cillum dolore eu fugiat nulla pariatur. Excepteur sint occaecat cupidatat non proident, sunt in culpa qui officia deserunt mollit anim id est laborum.



## Acknowledgments

I would like to thank all the members of my committee and my advisor Dr. Jingfeng Jiang. Their leadership, support, knowledge and motivation not only helped me throughout my research, but helped drive me to become a better scientist and to never stop learning.

Special thanks are also needed for Dr. Autumn Schumacher, who was willing to take a gamble on a brand new scientist fresh out of their undergraduate education. Her and expertise (and many hours of manuscript editing) were invaluable in getting me to where I am today.

I would also like to thank my friends for their boundless confidence in me which helped push me through my PhD work. Last but not the least, I would of course like to thank my family. All of their love and support helped make this thesis possible.



# Definitions

This provides information on how to write your MS thesis or PhD dissertation using the  $\text{\LaTeX}$  document preparation system in compliance with Michigan Technological University Graduate School requirements.

Lorem ipsum dolor sit amet, consectetur adipisicing elit, sed do eiusmod tempor incididunt ut labore et dolore magna aliqua. Ut enim ad minim veniam, quis nostrud exercitation ullamco laboris nisi ut aliquip ex ea commodo consequat. Duis aute irure dolor in reprehenderit in voluptate velit esse cillum dolore eu fugiat nulla pariatur. Excepteur sint occaecat cupidatat non proident, sunt in culpa qui officia deserunt mollit anim id est laborum.

Sed ut perspiciatis unde omnis iste natus error sit voluptatem accusantium doloremque laudantium, totam rem aperiam, eaque ipsa quae ab illo inventore veritatis et quasi architecto beatae vitae dicta sunt explicabo. Nemo enim ipsam voluptatem quia voluptas sit aspernatur aut odit aut fugit, sed quia consequuntur magni dolores eos qui ratione voluptatem sequi nesciunt.

Lorem ipsum dolor sit amet, consectetur adipisicing elit, sed do eiusmod tempor incididunt ut labore et dolore magna aliqua. Ut enim ad minim veniam, quis nostrud exercitation ullamco laboris nisi ut aliquip ex ea commodo consequat. Duis aute irure

dolor in reprehenderit in voluptate velit esse cillum dolore eu fugiat nulla pariatur. Excepteur sint occaecat cupidatat non proident, sunt in culpa qui officia deserunt mollit anim id est laborum.

Sed ut perspiciatis unde omnis iste natus error sit voluptatem accusantium doloremque laudantium, totam rem aperiam, eaque ipsa quae ab illo inventore veritatis et quasi architecto beatae vitae dicta sunt explicabo. Nemo enim ipsam voluptatem quia voluptas sit aspernatur aut odit aut fugit, sed quia consequuntur magni dolores eos qui ratione voluptatem sequi nesciunt.

Lorem ipsum dolor sit amet, consectetur adipisicing elit, sed do eiusmod tempor incididunt ut labore et dolore magna aliqua. Ut enim ad minim veniam, quis nostrud exercitation ullamco laboris nisi ut aliquip ex ea commodo consequat. Duis aute irure dolor in reprehenderit in voluptate velit esse cillum dolore eu fugiat nulla pariatur. Excepteur sint occaecat cupidatat non proident, sunt in culpa qui officia deserunt mollit anim id est laborum.

Sed ut perspiciatis unde omnis iste natus error sit voluptatem accusantium doloremque laudantium, totam rem aperiam, eaque ipsa quae ab illo inventore veritatis et quasi architecto beatae vitae dicta sunt explicabo. Nemo enim ipsam voluptatem quia voluptas sit aspernatur aut odit aut fugit, sed quia consequuntur magni dolores eos qui ratione voluptatem sequi nesciunt.

Lorem ipsum dolor sit amet, consectetur adipisicing elit, sed do eiusmod tempor incididunt ut labore et dolore magna aliqua. Ut enim ad minim veniam, quis nostrud exercitation ullamco laboris nisi ut aliquip ex ea commodo consequat. Duis aute irure dolor in reprehenderit in voluptate velit esse cillum dolore eu fugiat nulla pariatur. Excepteur sint occaecat cupidatat non proident, sunt in culpa qui officia deserunt mollit anim id est laborum.

Sed ut perspiciatis unde omnis iste natus error sit voluptatem accusantium doloremque laudantium, totam rem aperiam, eaque ipsa quae ab illo inventore veritatis et quasi architecto beatae vitae dicta sunt explicabo. Nemo enim ipsam voluptatem quia voluptas sit aspernatur aut odit aut fugit, sed quia consequuntur magni dolores eos qui ratione voluptatem sequi nesciunt.





## List of Abbreviations

ACA	Anterior Communicating Artery
AFI	Aneurysm Formation Indicator
CFD	Computational Fluid Dynamics
DICOM	Digital Imaging and Communications in Medicine
DVO	Degree of Volume Overlap
ENR	Elastic Net Regression
IA	Intracranial Aneurysm
ICA	Internal Carotid Artery
MCA	Middle Cerebral Artery
MLR	Multiple Logistic Regression
NSC	Nearest Shrunk Centroid
OSI	Oscillatory Shear Index
PC-MRI	Phase Contrast Magnetic Resonance Imaging
ROC	Receiver Operator Characteristic
STA-WSS	Spatiotemporally Averaged Wall Shear Stress
TA-WSS	Temporally Averaged Wall Shear Stress
VMTK	Vascular Modeling Toolkit
VTK	Visualization Toolkit

WSS	Wall Shear Stress
WSSG	Wall Shear Stress Gradient
$\lambda_2$	Lambda <sub>2</sub>
ACL	Access Control List
AIB	Add-In Board
ALE	Arbitrary Lagrangian Eulerian
AMANDA	Advanced Maryland Automatic Network Disk Archiver
AMBER	Assisted Model Building with Energy Replacement
AMD	Advanced Micro Devices
AMOLED	Active-Matrix Organic Light Emitting Diode
AMPI	Adaptive Message Passing Interface
ANL	Argonne National Laboratory
API	Application Program Interface
ASCII	American Standard Code for Information Interchange
ATLAS	Automatically Tuned Linear Algebra Software
b_eff	effective bandwidth Benchmark
BIOS	Basic Input/Output Operating System
BLAS	Basic Linear Algebra Subprograms
BOMD	Born-Oppenheimer Molecular Dynamics
BP	Bootstrap Protocol
CCSR	Center for Computer Systems Research

CentOS	Community enterprise Operating System
CFD	Computational Fluid Dynamics
CHARMM	Chemistry at HARvard Macromolecular Mechanics
CHAMBER	CHarmm $\leftrightarrow$ AMBER
CMake	Cross Platform Make
CODINE	Computing in Distributed Networked Environments
CP2K	Car-Parrinello 2000
CPMD	Car-Parrinello Molecular Dynamics
CPU	Central Processing Unit
CSS	Central Security Service
CTM	Chemical Transport Model
CUDA	Compute Unified Device Architecture
CUDPP	CUDA Data-Parallel Primitives Library
DAE	Differential Algebraic Equation
DARPA	Defense Advanced Research Projects Agency
DAE	Delay Differential Equation
DFT	Discrete Fourier Transform
DFT	Density Functional Theory
DGEMM	Double Precision GEneralized Matrix Multiplication
DHCP	Dynamic Host Configuration Protocol
DMCA	Digital Millennial Copyright Act

DOD	Department of Defense
DOE	Department of Energy
DRM	Distributed Resource Manager
DRMAA	Distributed Resource Manager Application API
EFF	Electron Force Field
EVL	Electronic Visualization Laboratory
FCA	Fabric Collectives Accelerator
FEA	Finite Element Analysis
FFT	Fast Fourier Transform
FFTW	Fastest Fourier Transform in the West
FLOPS	Floating Point Operations per Second
FPU	Floating Point Unit
FSI	Fluid Structure Interaction
FTDT	Finite Difference Time Domain
FTP	File Transfer Protocol

# Abstract

This provides information on how to write your MS thesis or PhD dissertation using the  $\text{\LaTeX}$  document preparation system in compliance with Michigan Technological University Graduate School requirements.

Lorem ipsum dolor sit amet, consectetur adipisicing elit, sed do eiusmod tempor incididunt ut labore et dolore magna aliqua. Ut enim ad minim veniam, quis nostrud exercitation ullamco laboris nisi ut aliquip ex ea commodo consequat. Duis aute irure dolor in reprehenderit in voluptate velit esse cillum dolore eu fugiat nulla pariatur. Excepteur sint occaecat cupidatat non proident, sunt in culpa qui officia deserunt mollit anim id est laborum.

Sed ut perspiciatis unde omnis iste natus error sit voluptatem accusantium doloremque laudantium, totam rem aperiam, eaque ipsa quae ab illo inventore veritatis et quasi architecto beatae vitae dicta sunt explicabo. Nemo enim ipsam voluptatem quia voluptas sit aspernatur aut odit aut fugit, sed quia consequuntur magni dolores eos qui ratione voluptatem sequi nesciunt.

Lorem ipsum dolor sit amet, consectetur adipisicing elit, sed do eiusmod tempor incididunt ut labore et dolore magna aliqua. Ut enim ad minim veniam, quis nostrud exercitation ullamco laboris nisi ut aliquip ex ea commodo consequat. Duis aute irure

dolor in reprehenderit in voluptate velit esse cillum dolore eu fugiat nulla pariatur. Excepteur sint occaecat cupidatat non proident, sunt in culpa qui officia deserunt mollit anim id est laborum.

Sed ut perspiciatis unde omnis iste natus error sit voluptatem accusantium doloremque laudantium, totam rem aperiam, eaque ipsa quae ab illo inventore veritatis et quasi architecto beatae vitae dicta sunt explicabo. Nemo enim ipsam voluptatem quia voluptas sit aspernatur aut odit aut fugit, sed quia consequuntur magni dolores eos qui ratione voluptatem sequi nesciunt.

Lorem ipsum dolor sit amet, consectetur adipisicing elit, sed do eiusmod tempor incididunt ut labore et dolore magna aliqua. Ut enim ad minim veniam, quis nostrud exercitation ullamco laboris nisi ut aliquip ex ea commodo consequat. Duis aute irure dolor in reprehenderit in voluptate velit esse cillum dolore eu fugiat nulla pariatur. Excepteur sint occaecat cupidatat non proident, sunt in culpa qui officia deserunt mollit anim id est laborum.

Sed ut perspiciatis unde omnis iste natus error sit voluptatem accusantium doloremque laudantium, totam rem aperiam, eaque ipsa quae ab illo inventore veritatis et quasi architecto beatae vitae dicta sunt explicabo. Nemo enim ipsam voluptatem quia voluptas sit aspernatur aut odit aut fugit, sed quia consequuntur magni dolores eos qui ratione voluptatem sequi nesciunt.

# Chapter 1

## Introduction

Subarachnoid hemorrhage is a potentially devastating pathologic condition in which bleeding occurs into the space surrounding the brain. One of the prevalent conditions that may result in subarachnoid hemorrhage is the rupture of an intracranial aneurysm (IA). IAs are degenerative, irregular expansions of areas in the cerebral vasculature occurring in an estimated 3-5% of the global population [70, 141, 173]. Rupture of an IA can result in subarachnoid hemorrhage and affect an estimate 0.15% - 0.7% of the global population each year [82]. The mortality rates from ruptured IA are estimated between 45-50%, with survivors suffering significant neurological damage, including physical and cognitive impairment [115, 173]. Yet the disparity between the number of ruptured and unruptured IAs indicate that not all IAs are of danger. From a clinical perspective, improved medical imaging techniques have led to

an increase in the detection of unruptured IAs, and novel surgical intervention methods have aimed to reduce the instances of IA rupture and subarachnoid hemorrhage [103, 125]. Yet data has shown that the risk of treatment may carry the same level of risk, as well as similar impacts to morbidity and mortality, as the possibility of IA rupture [30, 113, 121]. Therefore, elucidating the processes and conditions which impact IA rupture and incorporating them into predictive measurement may benefit clinicians. In an optimal situation, clinicians could assess known IA rupture factors in a patient to determine if their IA is at a low risk of rupture, or at a high risk of rupture/in need of treatment. Research has shown that a wide array of risk factors may impact IA development, growth and rupture potential [42, 104, 134, 154], but these factors can generally be broken down into four categories:

- IA morphological characteristics
- Vascular hemodynamics
- Cellular biomechanical processes
- Patient genetic and health factors



## Morphological Characteristics

Morphological characteristics of IAs are oft-considered when determining their rupture potential. Factors such as IA size (volume), shape, aspect ratio, IA to parent vessel angles, etc. have been identified in a number of studies as impacting rupture potential. However, many of these parameters are shown to generate conflicting results between studies evaluating their strength in rupture prediction. As per example, IAs  $>7\text{mm}$  in size are often associated with rupture risk, with IAs  $>25\text{mm}$  thought to be at the greatest rupture risk. If applied clinically, this would leave many small IAs ( $<7\text{mm}$ ) untreated due to the thought that the risk of complications from surgical interventions is thought to be of greater risk than the possibility of small IA rupture. Yet small aneurysms have been shown to be at a non-insignificant risk of rupture [51] and not all large IAs rupture. The strength of IA size on rupture impact may be further complicated by IA location, which has also been noted to potentially impact IA rupture [178? ]. In addition to IA size, additional morphological characteristics are applied to clinical assessment of IAs, yet similar discrepancies exist between studies assessing their impact on rupture prediction.

## Hemodynamic Characteristics

Hemodynamic stressors are thought to be of significant impact on the initiation, growth and possible rupture of IAs. The highly variable hemodynamic environment directly impacts the cells along the vascular wall

The tangential fluid stressors along the vascular wall, known as wall shear stress (WSS), and its derivatives are of significant focus in IA research. These quantifiable forces have been shown to act as a biological stimulator, triggering vascular cell function and remodeling. This has led the foci of studies to assess WSS predictive strength for IA rupture. In a similar vein to morphological characteristics, discrepancies exist of to which hemodynamic characteristics should be applied to rupture prediction and their overall predictive strength. It has been shown that vascular cells maintain healthy physiological characteristics while exposed to a range of WSS between  $0$  and  $15$  dynes/cm<sup>2</sup>. Yet studies are in conflict if WSS lower [17, 124] or higher [43, 150] from the preferred range is of greater impact on vascular cells, with some work suggesting that both high and low WSS impact IAs but stemming from differing impacts on vascular cells [123]. Even focusing on one extrema of WSS values and their impact on IA rupture has proven difficult. In a 2016 meta analysis by Zhou, the impact of low wall shear stress on predicting IA rupture varied widely between studies (Fig. ??). Nonetheless, while the exact role of WSS and its impact

on IA rupture is still being elucidated, WSS has been shown to strengthen many rupture prediction studies. It is worth noting, that measurements of hemodynamic characteristics and WSS *in-vivo* is possible, yet remains difficult especially in smaller blood vessels and small IAs. Improvements in computational fluid dynamics (CFD) can help overcome the *in-vivo* limitations and is being adopted as a clinical tool for assessment of rupture potential and planning of IA treatments [156, 169].

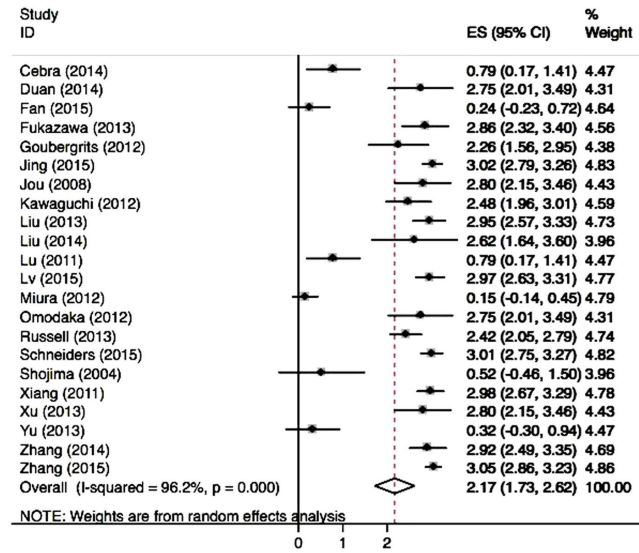


**Figure 1.1:** Zhou 2016 Meta-analysis of the reported low WSS rate of rupture aneurysms and the Odds Ratio for low WSS in predictive modeling

Current surgical interventions typically focus on occluding blood flow into an IA. IA clipping involves opening the skull to place a titanium clip around the opening (ostium) of the IA. Yet a meta-analysis between 1990 and 2011 showed this surgical methodology carried with it a 1.7% and 6.7% mortality and morbidity rate (respectively) [106]. A more recent method to repair IAs and prevent their potential rupture

is through coiling: the implantation of flexible platinum wires inside an IA to create an artificial thrombosis within the IA sac. A combination of coiling alongside implantation of a stent across the IA ostium may be used to help ensure proper coil retention within the IA sac. Treatment of IAs with coiling has been shown to have an 80-85% success rate [125], yet carries with it complication risks: morbidity, mortality, coil slippage, incomplete occlusion or coil compaction [80, 113]. While clinical intervention methods have been shown to reduce the onset of IA rupture, they are not without their own inherent physiological risk, leading to similar neurological damage as a ruptured IA[30, 113, 121].

Typically, the geometrical properties of IA and their surrounding vasculature as well as patient medical history and health factors (smoking, diabetes, etc) [8] have been linked with IA rupture. [155, 161]. Additionally, a growing body of research has focused on the hemodynamic stressors along the IA wall, and how they may contribute to the development of IAs and their and potential rupture, specifically how they trigger pathologic changes to vascular cells [10, 21, 27, 43, 111].

While a number of metrics (geometric, hemodynamic, and health factors) have alluded to IA rupture prediction, the strength of many of the individual metrics vary between studies [191]. F, and not all large IAs rupture. Additionally, the strength that hemodynamic stressors have on IA rupture potential varies between studies and both high and low wall shear stress have been suggested as being a predictive metric for

IA rupture by triggering varied cellular changes [123].

To better differentiate aneurysms at risk of rupture, novel assessment of the ever-changing hemodynamic conditions within the IA sac may hold the key. Flow patterns within aneurysm, specifically the swirling flow (vortices) in IAs, have been thought to impart pathologic cellular changes to vascular cells. Yet the presence of swirling flow patterns, or a visual, qualitative appraisal of flow complexity is what is typically correlated with IA rupture risk. The focus of this thesis is that by applying a novel analysis technique to assess the temporal changes to vortices' stability and complexity over the cardiac cycle and how they may be useful in identifying the possible development and rupture potential of cerebral IAs.

Lorem ipsum dolor sit amet, at qui viderer recusabo aliquando, dignissim evertitur ei his. Ignota iuvaret fabulas ei vim. Ne utinam inciderint quo. Pri ea congrue postulant conclusionemque. Ut elit dicam elaboraret pro, ius altera voluptaria cu. Eam mazim aliquip cu, recusabo pericula accommodare at mea, facer affert nonumes qui ea.

Discere dissentiet vel et, soluta nostrum epicurei ad eam, cu has aperiam vituperata. In prima quaeque diceret pri. Enim labores contentiones eos at, duo altera denique nominavi ea, eos inani nominavi consecutur at. Ut elit dicam elaboraret pro, ius altera voluptaria cu. Eam mazim aliquip cu, recusabo pericula accommodare at mea, facer affert nonumes qui ea. [37, 47, 49]

## Section 1

At vix indoctum disputando. Eam cu doctus reprimique, quaeque democritum an eos, sit veniam facete dissentias id. Tale volumus eos te, an eum nulla tincidunt. Mea id recteque theophrastus.

Eirmod malorum vis ei. Choro euismod incorrupte in vim, ludus ornatus vis ex. Hinc wisi impedit eum no, vocent definiebas referrentur in quo. Sanctus vulputate repudiandae usu ut.

## Objective

Although there exists a number of studies[22, 171, 191] and methodologies[55, 67] that attempt to assess IAs at a high risk of rupture, inconsistencies between study outcomes leave the development of an ideal predictive model out of reach. In addition, many of these previous studies assess the geometric[1, 96, 171] and/or hemodynamic wall stressors[22, 124, 191] as a means to predict IA rupture, with limited quantitative assessment of the hemodynamic flow conditions within the aneurysm. **The primary objective** of this work is to assess the viability of adapting quantitative analysis of hemodynamic flow patterns, specifically swirling flow pattern(s) (vortex), within IAs

to improve the prediction and understanding of IA rupture. In this work, an overview of recent theories concerning

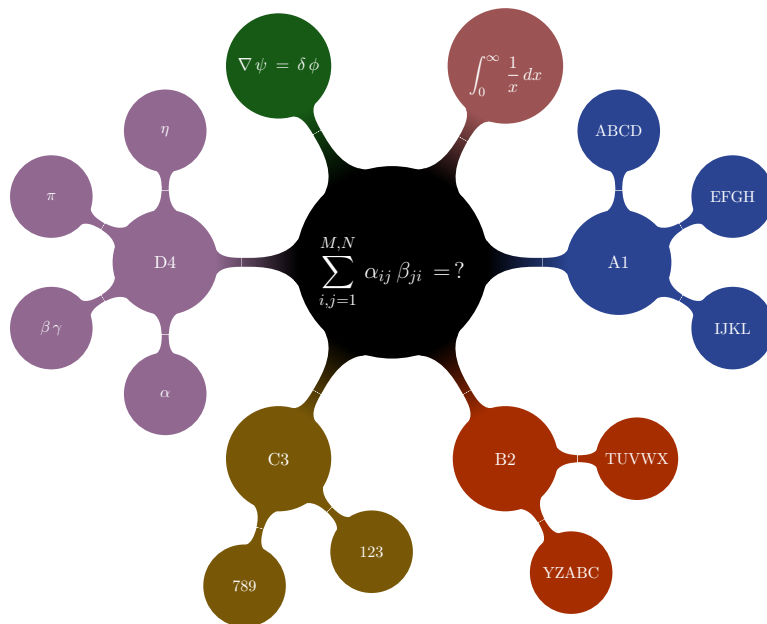


**Figure 1.2:** Schematic representation of our universe

## Methodology

For the initial focus of this work, image-based computational fluid dynamics models of patient-specific IA geometry will be constructed from 3D phase contrast magnetic resonance imaging (PC-MRI). Computational fluid dynamic (CFD) simulations will be performed on the computational models to generate realistic 3D hemodynamic velocity and flow pattern data. From said data,

Simul noster voluptaria eam ei, sint regione pri ei. Cum no utinam equidem, falli

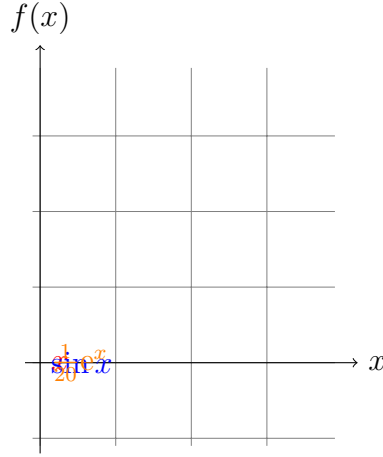


**Figure 1.3:** Mathematical functions plotted using TikZ package

bonorum prodesset an qui. Alterum dissentiet vituperatoribus te eam, eos ea suas oblique. Per ea utinam facilisi. [38, 45, 46] Per iudico probatus complectitur et, cum tollit atomorum rationibus ea.

## Aneurysm Geometric Characteristics

All aneurysm geometries were taken from the finalized computational mesh generated for simulations. The aneurysm sac was manually isolated from the parent vessel and the resultant cut plane was capped and identified as the IA ostium using an in-house script written in VMTK. Geometric measurements were either taken directly from the values reported in the Aneurisk dataset, or were calculated using in-house scripts in VMTK.



Aneurysm Surface Area and Volume: Measured directly from the isolated IA geometry before and after (respectively) ostium capping. A number of studies have eluded to an increase in IA size as a risk for both IA growth and rupture. [8, 18, 67, 171]. A meta-analysis performed by Brinjikji et al reported that IA  $\leq 10$  mm in size (diameter) grew at a rate  $< 2.9\%$  per year, while IAs  $> 10$  mm were associated with growth rates of  $9.7\%$  per year. This growth was also reported with an associated IA rupture rate:  $3.1\%$  per year compared with  $0.1\%$  per year for stable (non-growing) aneurysms ( $p \leq 01$ ). From a clinical perspective, the overall size of an aneurysm is often a characteristic used to determine course of IA treatment (or lack thereof) [103, 180]. Yet while large IAs are thought to increase the likelihood of rupture, a not-insignificant number of small IAs ( $< 5$  mm diameter) also have been shown to rupture [92, 96, 104]. This disparity between sizes of ruptured IAs suggest that the assessment of additional factors in tandem with IA size may improve rupture prediction.

Aneurysm Height: The length of the centerline of the IA sac is measured, following the IA shape, as opposed to measuring a straight line from the ostium centroid directly to the highest IA point. The radius of the maximum inscribed sphere at the centerline's furthest point is added to the length measurement to fully measure the IA height. This is a modified version of the typical IA height measurement: a straight line of the maximum stretch from the ostium centroid to the IA dome [51, 117].

Vessel Diameter: The parent artery diameter value is computed at locations close to

the aneurysm ostium. For terminal aneurysms, the vessel diameter of the common branch was measured at the point prior to centerline splitting between the daughter arteries, and both daughter arteries' diameter were measured at the point one (common artery) diameter away from the IA ostium cut. The average of the three values was used as the value of the vessel diameter.

Inlet Cross-sectional Area: The beginning of the inlet vessel was cut square in the 3-matic software package, the resultant cross-sectional area of the inlet vessel was calculated.

Aspect Ratio\*: A modified calculation of the commonly defined aspect ratio (aneurysm hight/ostium diameter) was used by adapting the sac centerline (SC) length as a measure of aneurysm height as well as taking into account the area and circumference of the ostium since the diameter of the ostium is rarely uniform for the whole ostium [135].

$$AspectRatio* = (SC_{length} / (4 * (Ostium_{area} / Ostium_{circumfrence}))) \quad (1.1)$$

The aspect ratio of an IA has been shown to be correlated with levels of hemodynamic stressors and has been used as an ease-of-use method to assess conditions within an IA.

# Aneurysm Hemodynamic Characterisitcs

Wall Shear Stress: The calculation of wall shear stress (WSS) is performed by the ANSYS-FLUENT commercial finite-element solver (ANSYS v17.0). The value is defined as the normal velocity gradient against the (vessel) wall:

$$\tau_w = \mu \frac{\partial v}{\partial n} \quad (1.2)$$

with  $\mu$  as the fluid dynamic viscosity (0.004 kg/m-s).

The spatial-temporally averaged value of the aneurysm's WSS was calculated alongside its temporally-averaged WSS minimum and temporally-averaged WSS maximum. In a similar manner as IA volume, research differs on whether high [43] or low [189] wall shear stress is a better predictive metric for IA rupture potential. In a study by Meng et. al., both high and low WSS were associated with IA rupture potential, yet causing differing cellular changes [123].

Kinetic Energy Density: The kinetic energy density (KED) within the IA dome was calculated as follows:

$$KED = \frac{\frac{1}{2}\rho \sum v^2}{n} \quad (1.3)$$

Where  $v$  is the velocity values,  $\rho$  is the mass density of blood, and  $n$  is the number

of voxels within the IA. The KED at each time-step (along the cardiac phase) was calculated, as well as the Temporally averaged KED (TA-KED) for all cases.

## **Disturbed Flow on Vascular Endothelium**

The vascular endothelial cell (EC) layer forms the innermost lining of blood vessels, directly interacting with hemodynamic stressors and helping to maintain homeostatic functions of the vasculature[33, 91]. The mechanotransduction capabilities of this initial vascular layer help maintain a selective macromolecular barrier, trigger vascular remodeling, regulate vascular smooth muscle cell contraction[170], and help control vascular inflammatory responses[28]. The degradation of vascular homeostasis, resultant from disturbed hemodynamic flow patterns, has been associated with an array of vascular pathologies: aneurysms[25, 115], atherosclerosis[114], and thrombosis[34, 168]. Due to the life threatening nature of IAs, improved quantitative methods to characterize hemodynamic patterns and to what degree they impart EC pathologic changes, could prove essential to further our understanding of the disease's initiation and progression.

The morphology and cytoskeletal organization of EC have been shown to be susceptible to non-laminar flow conditions[175]. Typically, EC morphology aligns along flow directionality, forming organized parallel actin stress fibers and giving the cells

an elongated structure[11, 91, 160]. Disrupted flow patterns resulting in vortex flow and altered WSS, show a differential change in EC characteristics: a rounded morphology with marginally located short actin stress fibers[34, 44, 168]. These changes have been associated with a number of structural-functional changes in vascular cells, such as increased permeability to macromolecules, increased expression of adhesion molecules (ICAM-1, VCAM-1), decreased endothelial cell regeneration and increased smooth muscle cell proliferation/migration.

Additionally, inflammatory processes within vasculature has been shown to be a significant actor in the pathogenesis of IA development and potential rupture [28, 76, 152]. In a typical physiological setting, the vascular EC layer maintains antiatherogenic characteristics, inhibiting platelet adhesion and aggregation along the vascular wall, as well as limiting cellular pro-inflammatory pathways[3]. In the occurrence of IA pathology, a breakdown of the EC inflammatory-limiting capabilities is noted: small aneurysm shown to have intimal thickening and diffuse macrophage/lymphocyte infiltration, whereas chronic atherosclerotic lesions with embedded macrophages and lymphocytes have been noted in larger aneurysms[105, 167]. Upon leukocyte and macrophage infiltration, the matrix metalloproteinase enzyme is released which digests extracellular matrix proteins leading to additional pathologic damage to the vascular wall[6, 164]. The remodeling of the vascular wall, impart due to inflammatory pathogenic activities, lead to an overall loss vessel mechanical strength and a possible ballooning out of the impacted area

Docendi eligendi sit et, pri ea dicam eligendi percipitur, has soleat dolores convenire te. Sed altera placerat an, id verterem abhorreant interesset mea. Eum at ceteros efficiantur. Eos id voluptaria efficiendi comprehensam. [47, 48]

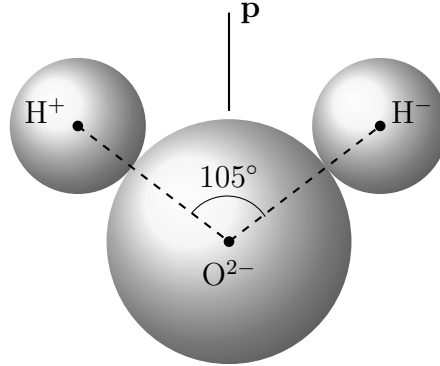


**Figure 1.4:** Schematic representation of a water molecule

In mel modo dicam vocibus, eruditi consecutuer vim no, cu quaestio instructor eum. Justo nostrud fuisset ea mea, eam an libris repudiandae vituperatoribus. Est choro corrumpit definitionem at. Vel sint adhuc vocibus ea, illud epicuri eos no. Sea simul officiis ea, et qui veri invidunt appellantur. Vix et eros ancillae pertinax. [56, 65, 66, 78, 136] Per iudico probatus complectitur et, cum tollit atomorum rationibus ea. Per iudico probatus complectitur et, cum tollit atomorum rationibus ea.

Aliquip lobortis ei est, at error viris graeco sed. Vel te elitr detracto, modo graecis scripserit ex nec. Errem utamur viderer per no, eam ea eripuit referrentur. Pro te dicat disputando. Per iudico probatus complectitur et, cum tollit atomorum rationibus ea. [130, 140, 144, 153]. Per iudico probatus complectitur et, cum tollit atomorum rationibus ea.

Per iudico probatus complectitur et, cum tollit atomorum rationibus ea. Docendi eligendi sit et, pri ea dicam eligendi percipitur, has soleat dolores convenire te. Per iudico probatus complectitur et, cum tollit atomorum rationibus ea.





## Chapter 2

# Hemodynamic Flow Vortex Identification

Recent attention has focused on assessing hemodynamic characteristics as disturbed aneurysmal hemodynamics is known to have an impact on the origin and natural history of IAs [19, 177]. From a clinical perspective, phase-contrast magnetic resonance imaging (PC-MRI) or Phase-contrast magnetic resonance angiography (PC-MRA) has been used to assess flow characteristics in the vasculature *in-vivo* [15, 122]. Yet, determining flow details in and around IAs has proven difficult with PC-MRI/PC-MRA. The individual protons in complex and disturbed aneurysmal flow has incoherent velocities (at the sub-grid level) and these specific characteristics cannot be

resolved by a typical "averaged" velocity measurement from a relatively large resolution cell (*at 1-mm scale*). The consequence of this sub-grid limitation, clinical hemodynamic flow measurements may be impacted by errors and potential flow artifacts which adversely affect the accuracy of PC-MRI/PC-MRA results. In parallel to research efforts of assessing MR flow imaging in and around IAs to determine rupture characteristics, blood flow simulated from "patient-specific" computational fluid dynamics (CFD) simulations [156] have also garnered interest by the clinical and research community [26, 182]. CFD simulation data has an initial advantage over MRI derived data in that a high degree of control of both desired data resolution, as well as data quality (lack of imaging errors and flow artifacts) can be maintained. The development of novel flow measurement techniques can be initially created and tested on data free from errors which may confound initial findings.

Assessment of hemodynamic conditions from CFD simulations has brought about a number of potential parameters that correlate to IA rupture risk: wall shear stress [10], oscillatory shear index [157], flow impingement [26], and flow stability [21]. As mentioned in the focus of flow stability, Bryne et al. [21] found that aneurismal flow that aligns with IA rupture is closely correlated with flow spatial complexity and temporal stability. Yet this methodology only relies on the assessment of the centroid-most region of vortex patterns (vortex core), giving less insight on the broader structural changes to vortices. Expanding upon the idea of vortex analysis to identify, and quantify changes to, the broader structure of vortices may give additional insight into

flow characteristics that can be linked to IA rupture potential.

In an initial study, the development of an alternative technique that expanded upon vortex core analysis was investigated to characterize the presence, destruction and motion of vortices within an IA [159]. This image processing algorithm expanded upon two established vortex identification methods, the  $Q$ -criterion [84] and  $\lambda_2$  [88] methods, to identify and assess the broader aspects of vortices as opposed to solely identifying the vortex core. Subsequent studies investigated the use of a vortex identification methodology based on the Shannon’s entropy (CITATION NEEDED) as an alternative identification metric not wholly reliant upon vortex core identification.

Due to the differences between traditional CFD data resolution (high) and MRI derived flow data (lower resolution), the identification methods were based on velocity data on a rectilinear grid, and the susceptibility of changes to vortex identification outcomes were tested under a range of grid resolutions. Additionally, variations to methodological outputs were tested under a range of chosen threshold values (dependent on the method and will be explained in Section NEED THE SECTION). The vulnerability of a methodology to significant changes in outcomes with minimal changes to methodological threshold values could in theory result in variations to research findings if differing thresholds were to be applied to a wide array of studies. Toward this end, the primary focus of this work was to explore analyzing the spatio-temporal characteristics of hemodynamic vortices as a possible means to compliment

future assessment of IA rupture potential.

## Materials and Methods

### Modeling of "Patient-specific" Vasculature

In the initial study 10 cases of IAs were arbitrarily selected from an internal database: five cases with a single terminal aneurysm, and five cases with a single sidewall aneurysm. Models were either located within the internal carotid artery or the basilar artery. A commercially available image segmentation package (Mimics Innovation Suite, version 17, Materialise Inc. Leuven, Belgium) was used to reconstruct the vascular surface from digital subtraction angiography (DSA) scans. For all cases, the longest possible upstream section proximal to the aneurysm, was left intact to maintain as much of the patient vessel as possible. Surface irregularities were removed using the 3-matic software (Version 9, Materialize Inc., Leuven, Belgium) as well as a 1<sup>st</sup> order Laplacian smoothing filter to reduce irregularities while preserving vascular geometry. Cylindrical flow extensions (6 times the inlet vessel diameter) were added to each model using the open-source Vascular Modeling Toolkit (VMTK) software (version 1.2). The addition of vessel extensions help reduce the effects of inlet, plug-flow flow on hemodynamic characteristics [137].

## Mesh Generation

Processed vascular surface structures were converted into an unstructured, 3D, tetrahedralized volumetric mesh using an open-source mesh generator, Tetgen (version 1.4.2) [151]. The mesh generation process was done by an in-house Python script derived from the VMTK program. Approximately, 1 million computing cells were used per case, with the average mesh size as  $0.0022\text{-mm}^3$ .

## CFD Simulation

To compute fluid velocity waveforms in and around the IA, the time-dependent incompressible, 3D Navier-Stokes equations for the meshed vessel geometry was solved using two CFD solvers: a commercial CFD solver (version 14.0, ANSYS-FLUENT Inc., Lebanon, NH) and a research prototype CFD solver (version 4.0, Siemens Medical Solution Inc., IL). Details on the Navier-Stokes equation can be found in the Appendix. In the ANSYS-FLUENT solver, the pressure-velocity coupling was obtained using the SIMPLEC algorithm [172]. The explicit time-marching second-order scheme with a time step of  $1 \times 10^{-3}$  second (1000 steps per cardiac cycle) was used for computations.

As the Siemens research CFD solver is still under development, limited information on

its methods for solving the Navier-Stokes equation will be discussed in this thesis. IA models were defined by water-tight 3D surface triangles were automatically discretized with cubical voxels. A Lattice-Boltzmann Method (LBM) solver was then used to choose adaptively choose the solver time-step, and varied from  $1 \times 10^{-3}$  to  $2 \times 10^{-3}$ . A Siemens Leonardo workstation equipped with a dual quad-core CPU and 8 GB of memory was used to perform CFD simulations. Of note, the exact same vessel geometries (STL files) were used to generate the volumetric meshes (for the ANSYS-FLUENT solver) and voxel discretization (for the LBM solver). The final velocity results obtained from the LBM method were resampled to form velocity data onto a rectilinear grid whose voxel size varied from 0.18 to 0.25 mm.

In both solvers, vessels walls were assumed rigid with a no-slip boundary. Blood was considered an incompressible and Newtonian fluid with a dynamic viscosity of 0.004 kg/m-s and a mass density of 1050 kg/m<sup>3</sup>. A zero-pressure condition was used for all vessel outlets. For inlet flow rates, two pulsatile waveforms at a rate of 60 bpm were derived from magnetic resonance measurements and were taken from Gwilliam et al. [69] as patient-specific flow waveforms were not available. Each case had its inlet waveform scaled according to their inlet cross-sectional area, standardizing their mean volumetric flow rate to either 280mL/min for ICA cases or 180mL/min for BAs. This choice of volumetric flow rate(s) were based on measured physiological flow rates available in MR literature [54, 190]. Four (4) cardiac cycles were simulated per case at 20 data points per cardiac cycle with only the final cardiac cycle saved as a means

to reduce initial transient flow conditions.

## **Aneurysm Extraction and Voxelization of Aneurismal Velocity Data**

A published method [89] was used to semi-automatically isolate and extract the IA sac. The isolated IA sac was sealed at the IA opening (ostium) and converted to a binary mask that is spatially-registered with the volumetric velocity data. The mask allows the analysis of only the intra-aneurysmal velocity data. TO verify intra-rater reliability of proper sectioning of IA masks, 2 separate users sectioned the IAS and Bland-Altman plots were performed on the resultant mask volumes and ostium areas to determine the similarity between chosen masks. Once no significant differences were ensured between sectioned masks, one user was chosen at random and all resultant masks from that user were implemented in the rest of the study.

## **Vortex Core Extraction and Analysis**

All computational methods for identification and extraction of vortices and spatio-temporal analysis of said vortices were performed using in-house scripts (C++ and Python) that were derived from the open-source VTK/VMTK software package.

This flow assessment was performed through the analysis of vortex critical point (core) lines and it was concluded that "ruptured aneurysms had more complex and more unstable flow patterns than un-ruptured aneurysms." In their work, Bryne used proper orthogonal decomposition [] of time-resolved velocities were used to characterize temporal flow stability. As a brief explanation, vortex core lines, identifying the center-most region of vortex pattern, were identified by the use of a co-linearity conditions between flow instantaneous vorticity  $\vec{\omega}$  and velocity  $\vec{v}$  vectors.

$$\begin{aligned}\vec{\omega} \times \vec{v} &= 0 \\ \vec{\omega} &= \nabla \times \vec{v}\end{aligned}\tag{2.1}$$

To identify the centroid region of vortices, the eigenvalues of the velocity gradient tensor was calculated. In the event of a pair of complex conjugate eigenvalues was identified, the vorticity vector  $\vec{\omega}$  as calculated and tested against the velocity vector to assess whether Equation 2.1 was satisfied. From an identified element, the velocity component in the direction of vorticity vector was subtracted from the velocity vector (reduced velocities). Element faces that had a point where the reduced velocity is zero was marked, and if two or more faces of an element had a zero reduced velocity, a vortex core line passes through the element.

Vortex core line analysis



$$\nabla \vec{u} = S + \Omega$$

$$S = \frac{1}{2} [(\nabla \vec{u}) + (\nabla \vec{u})^T] \quad (2.2)$$

$$\Omega = \left[ \frac{1}{2} (\nabla \vec{u}) - (\nabla \vec{u})^T \right]$$

Where  $\nabla \vec{u}$  is the calculation of the velocity gradient:  $S$  as the rate-of-strain tensor and  $\Omega$  as the vorticity tensor.

Hunt, Wray and Moin [84] defined a vortex as the spatial region of flow where the Euclidean norm of the vorticity tensor dominates.

$$Q = \frac{1}{2} [|\Omega|^2 - |S|^2] > 0 \quad (2.3)$$

Jeong and Hussain identified the vortices as:

$$\lambda_2 = (S^2 + \Omega^2) < 0 \quad (2.4)$$

where  $\lambda_2 A$  identifies a vortex when the second intermediate eigenvalue of the 3 x 3 tensor  $A$  is symmetric (all three eigenvalues are real).

In our original study, the normalized  $Q$  and  $\lambda_2$  values were tested to identify vortices within IAs.

$$Q(x, t) = \frac{Q(x, t)}{|\vec{u}(x, t)|^2} \quad (2.5)$$

$$\lambda_2(x, t) = \frac{\lambda_2(x, t)}{|\vec{u}(x, t)|^2}$$

Eirmod malorum vis ei. Choro euismod incorrupte in vim, ludus ornatus vis ex. Hinc wisi impedit eum no, vocent definiebas referrentur in quo. Sanctus vulputate repudiandae usu ut. In prima quaeque diceret pri. Enim labores contentiones eos at, duo altera denique nominavi ea, eos inani nominavi consecetuer at.

Liber liberavisse nec at, movet albucius principes has at. Ea sed persius accusam, clita sententiae adversarium ne sed. Usu no graecis theophrastus delicatissimi, sint aliquam an eam. Mei elit mnesarchum dissentias te, in essent laboramus per. Affert mucius quidam mel ex, per dicam insolens ad.

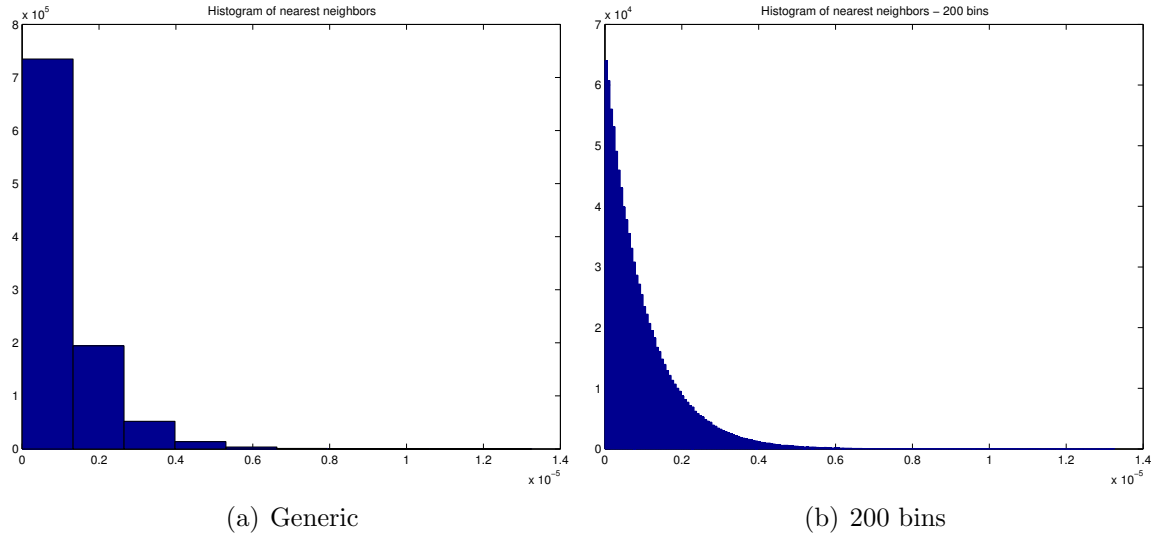


**Figure 2.1:** Histogram of nearest neighbors

Docendi eligendi sit et, pri ea dicam eligendi percipitur, has soleat dolores convenire te. Sed altera placerat an, id verterem abhorreant interesset mea. Eum at ceteros efficiantur. Eos id voluptaria efficiendi comprehensam.

In mel modo dicam vocibus, eruditi consecetuer vim no, cu quaestio instructior eum. Justo nostrud fuisset ea mea, eam an libris repudiandae vituperatoribus. Est choro corrumpit definitionem at. Vel sint adhuc vocibus ea, illud epicuri eos no. Sea simul officiis ea, et qui veri invidunt appellantur. Vix et eros ancillae pertinax.

Aliquip lobortis ei est, at error viris graeco sed. Vel te elitr detracto, modo graecis scripserit ex nec. Errem utamur viderer per no, eam ea eripuit referrentur. Pro te dicat disputando.

As explained in Table 2.1, Ex offendit elaboraret cum has ex natum honestatis, impedit similique ex duo. Et mei mollis scripta, et vim labores phaedrum, in cum facete saperet. Splendide elaboraret comprehensam qui ne. Putant verterem no vim, mea solum veritus definitiones ei, no labitur propriae deseruisse est. Ius illud everti salutandi id, eu facer pericula principes est.

Simul noster voluptaria eam ei, sint regione pri ei. Cum no utinam equidem, falli bonorum prodesset an qui. Alterum dissentiet vituperatoribus te eam, eos ea suas oblique. Per ea utinam facilisi. Per iudico probatus complectitur et, cum tollit

**Table 2.1**

A portrait table: first column represents the year in which the Nobel prize in physics was awarded; second column indicates the name of the scientist and the third column is the work for which the Nobel prize was awarded

Year	Scientist(s)	Nobel Work
1901	W. C. Röntgen	X-rays
1902	H. A. Lorentz	Influence of magnetism on radiation
	P. Zeeman	Influence of magnetism on radiation
1903	A. H. Becquerel	Spontaneous radioactivity
	M. Curie	Radiation phenomena discovered by Becquerel
	P. Curie	Radiation phenomena discovered by Becquerel
1904	J. W. Strutt	Argon
1905	P. E. A. von Lenard	Cathode rays
1906	J. J. Thomson	Electrical conductivity of gases
1907	A. A. Michelson	Spectroscopic and metrological investigations
1908	G. Lippmann	Photographic reproduction of colours
1909	K. F. Braun	Wireless telegraphy
	G. Marconi	Wireless telegraphy
1910	J. D. van der Waals	Equation of state of gases and liquids
1911	W. Wien	Laws governing heat radiation
1912	N. G. Dalèn	Automatic regulators for lighting coastal beacons and light buoys

atomorum rationibus ea.

Docendi eligendi sit et, pri ea dicam eligendi percipitur, has soleat dolores convenire te. Sed altera placerat an, id verterem abhorreant interesset mea. Eum at ceteros efficiantur. Eos id voluptaria efficiendi comprehensam.

Simul noster voluptaria eam ei, sint regione pri ei. Cum no utinam equidem, falli bonorum prodesset an qui. Alterum dissentiet vituperatoribus te eam, eos ea suas oblique. Per ea utinam facilisi. Per iudico probatus complectitur et, cum tollit atomorum rationibus ea.

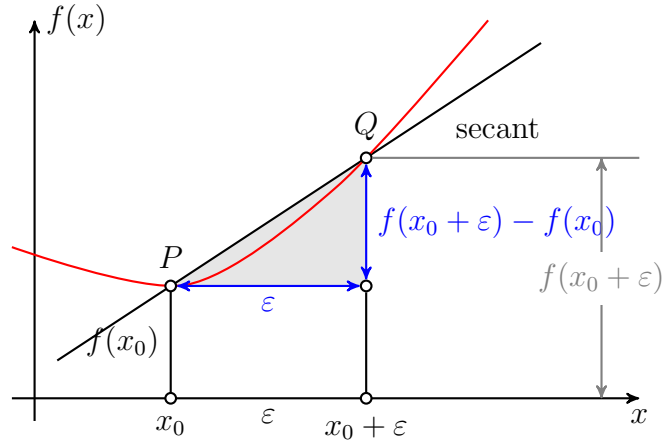


**Figure 2.2:** Fancy mathematical plots using TikZ package

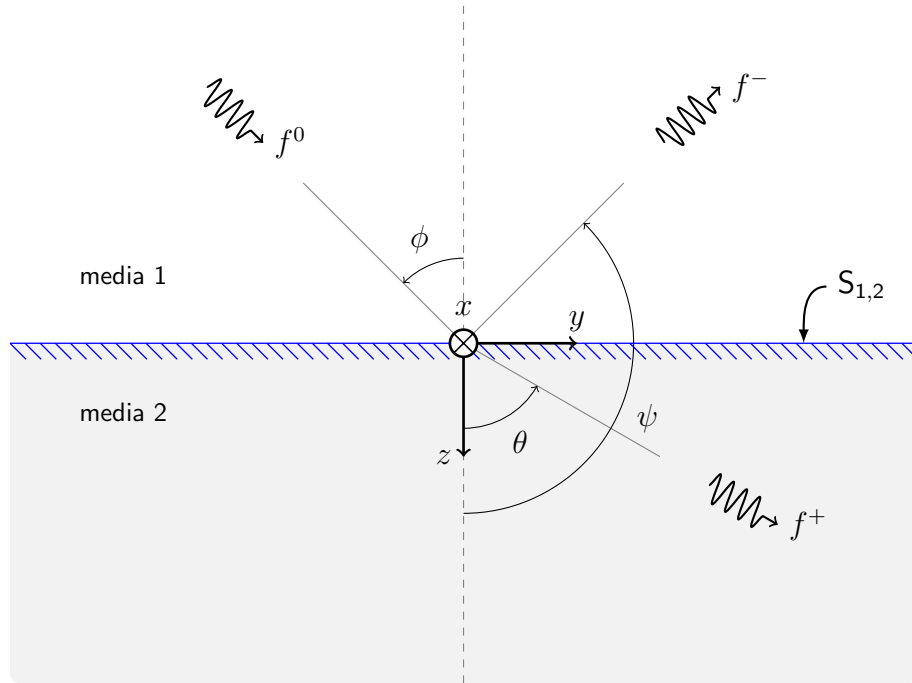


**Figure 2.3:** Incidence, transmission and reflection

Docendi eligendi sit et, pri ea dicam eligendi percipitur, has soleat dolores convenire te. Sed altera placerat an, id verterem abhorreant interesset mea. Eum at ceteros efficiantur. Eos id voluptaria efficiendi comprehensam. Simul noster voluptaria eam

ei, sint regione pri ei. Cum no utinam equidem, falli bonorum prodesset an qui.

# Chapter 3

## Vortex Analysis to predict IA Initiation

The tangential, frictional stress caused by blood flowing along the vessel wall is known as WSS. The ANSYS-FLUENT software calculates WSS by the normal velocity gradient at the vessel wall:

$$\tau_w = \mu \frac{\partial v}{\partial n} \quad (3.1)$$

where  $\mu$  is the dynamic viscosity. In this work, areas of high WSS were of interest as it is thought to play a role in the IA initiation [123]. High WSS was defined as values  $\geq 20$  Pa during peak systole of the MRI waveform.

The WSSG was calculated using in-house VMTK scripts and is derived from three

spatial derivatives of the WSS as follows:

$$WSSG = \sqrt{\left(\frac{\partial \tau_w}{\partial x}\right)^2 + \left(\frac{\partial \tau_w}{\partial y}\right)^2 + \left(\frac{\partial \tau_w}{\partial z}\right)^2} \quad (3.2)$$

with the time-averaged WSSG calculated as

$$WSSG_{av} = \frac{1}{T} \int_0^T |WSSG| dt \quad (3.3)$$

OSI is a nondimensional parameter, computing oscillations in the direction of the WSS vectors over the course of a cardiac cycle:

$$OSI = \frac{1}{2} \left\{ 1 - \frac{|\int_0^T \tau_i dt|}{\int_0^T |\tau_i| dt} \right\} \quad (3.4)$$

where  $\tau_i$  represents the WSS vector at a given time step across the duration of the cardiac cycle (T). The OSI describes the changes of a WSS vector's alignment with the cardiac cycle's temporally-averaged WSS vector. An OSI of 0 indicates no change in directionality and 0.5 being a complete direction reversal.

The AFI [?] quantifies the variation in angle between the instantaneous WSS vector and time-averaged WSS vector:

$$AFI = \cos(\theta) = \frac{\tau_i \cdot \tau_{av}}{|\tau_i| * |\tau_{av}|} \quad (3.5)$$



For each point along the vessel wall, the minimum AFI calculated during the cardiac cycle was used to indicate the greatest deviation of the WSS vector from its mean direction. A minimum AFI of -1, 0, and 1 indicate deviations of 180°, 90°, and 0° respectively.

The GON index [?] quantifies fluctuations in WSSG directionality over the cardiac cycle.

$$GON = 1 - \frac{|\int_0^T G dt|}{\int_0^T |G| dt} \quad (3.6)$$

T is the period of the cardiac cycle and G is the spatial wall shear stress gradient vector

Lorem ipsum dolor sit amet, at qui viderer recusabo aliquando, dignissim evertitur ei his. Ignota iuaret fabulas ei vim. Ne utinam inciderint quo. Pri ea congue postulant conclusionemque. In prima quaeque diceret pri. Enim labores contentiones eos at, duo altera denique nominavi ea, eos inani nominavi consecetur at. Ut elit dicam elaboraret pro, ius altera voluptaria cu.

Discere dissentiet vel et, soluta nostrum epicurei ad eam, cu has aperiam vituperata. In prima quaeque diceret pri. Enim labores contentiones eos at, duo altera denique nominavi ea, eos inani nominavi consecetur at. Ut elit dicam elaboraret pro, ius altera voluptaria cu. Eam mazim aliquip cu, recusabo pericula accommodare at mea, facer affert nonumes qui ea. [4, 62]

$$\begin{aligned}
d\nu_\theta &= \frac{N}{V} \left( \frac{m}{2\pi kT} \right)^{3/2} \left[ \int_0^{2\pi} \int_0^\infty v^3 e^{-mv^2/2kT} dv d\phi \right] \sin \theta \cos \theta d\theta \\
&= 2\pi \frac{N}{V} \left( \frac{m}{2\pi kT} \right)^{3/2} \left[ \int_0^\infty v^3 e^{-mv^2/2kT} dv \right] \sin \theta \cos \theta d\theta
\end{aligned}$$

At vix indoctum disputando. Eam cu doctus reprimique, quaeque democritum an eos, sit veniam facete dissentias id. Tale volumus eos te, an eum nulla tincidunt. Mea id recteque theophrastus.

$$d\nu_\theta = \frac{N}{V} \left( \frac{2kT}{m\pi} \right)^{1/2} \sin \theta \cos \theta d\theta \quad (3.7)$$

Liber liberavisse nec at, movet albucius principes has at. Ea sed persius accusam, clita sententiae adversarium ne sed. Usu no graecis theophrastus delicatissimi, sint aliquam an eam. Mei elit mnesarchum dissentias te, in essent laboramus per. Affert mucius quidam mel ex, per dicam insolens ad.

Sed altera placerat an, id verterem abhorreant interesset mea. Eum at ceteros efficiantur. Eos id voluptaria efficiendi comprehensam. Continuing from Eqn. (3.7)

$$\begin{aligned}
d\nu_v &= \frac{N}{V} \left( \frac{m}{2\pi kT} \right)^{3/2} \left[ \int_0^{2\pi} \int_0^{\pi/2} \sin \theta \cos \theta d\theta d\phi \right] v^3 e^{-mv^2/2kT} dv \\
&= 2\pi \frac{N}{V} \left( \frac{m}{2\pi kT} \right)^{3/2} \left[ \int_0^{\pi/2} \sin \theta \cos \theta d\theta \right] v^3 e^{-mv^2/2kT} dv
\end{aligned}$$

In mel modo dicam vocibus, eruditi consecetuer vim no, cu quaestio instructor eum. Justo nostrud fuisset ea mea, eam an libris repudiandae vituperatoribus. Est choro corrumpit definitionem at. Vel sint adhuc vocibus ea, illud epicuri eos no. Sea simul officiis ea, et qui veri invidunt appellantur. Vix et eros ancillae pertinax.

In mel modo dicam vocibus, eruditi consecetuer vim no, cu quaestio instructor eum. Justo nostrud fuisset ea mea, eam an libris repudiandae vituperatoribus. Est choro corrumpit definitionem at. Vel sint adhuc vocibus ea, illud epicuri eos no. Sea simul officiis ea, et qui veri invidunt appellantur. Vix et eros ancillae pertinax.

$$d\nu_v = \frac{N}{V} \pi \left( \frac{m}{2\pi kT} \right)^{3/2} v^3 e^{-mv^2/2kT} dv \quad (3.8)$$

Aliquip lobortis ei est, at error viris graeco sed. Vel te elitr detracto, modo graecis scripserit ex nec. Errem utamur viderer per no, eam ea eripuit referrentur. Pro te dicat disputando.

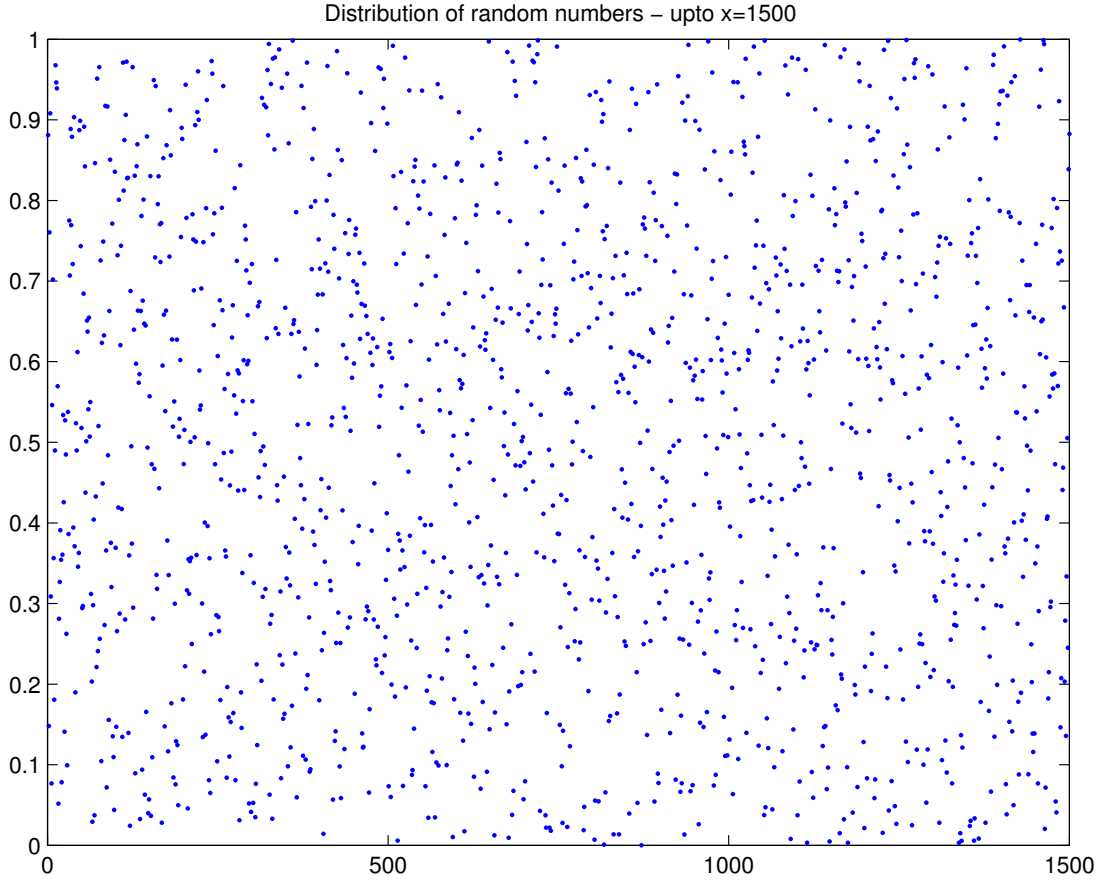


**Figure 3.1:** Distribution of random numbers

**Table 3.1**

Measured data points representing the relationship between  $x$  and  $y$

$x$	0	1	2	3	4	5	6	7	8	9	10
$y$	0	0.94	0.99	-0.52	-1.82	-0.44	3.54	6.69	5.38	0.00	-4.42

Et mei mollis scripta, et vim labores phaedrum, in cum facete saperet. Splendide elaboraret comprehensam qui ne. Putant verterem no vim, mea solum veritus definitiones ei, no labitur propriae deseruisse est. Ius illud everti salutandi id, eu facer pericula principes est.

**Table 3.2**

A landscape table: first column represents the year in which the Nobel prize in physics was awarded; second column indicates the name of the scientist and the third column is an *as is* Nobel citation

Year	Scientist(s)	Nobel Work
1901	W. C. Röntgen	in recognition of the extraordinary services he has rendered by the discovery of the remarkable rays subsequently named after him
1902	H. A. Lorentz and P. Zeeman	in recognition of the extraordinary service they rendered by their researches into the influence of magnetism upon radiation phenomena
1903	A. H. Becquerel	in recognition of the extraordinary services he has rendered by his discovery of spontaneous radioactivity
	M. Curie and P. Curie	in recognition of the extraordinary services they have rendered by their joint researches on the radiation phenomena discovered by Prof. Henri Becquerel
1904	J. W. Strutt	for his investigations of the densities of the most important gases and for his discover argon in connection with these studies
1905	P. E. A. von Lenard	Cathode rays
1906	J. J. Thomson	Electrical conductivity of gases
1907	A. A. Michelson	Spectroscopic and metrological investigations
1908	G. Lippmann	Photographic reproduction of colours
1909	K. F. Braun and G. Marconi	Wireless telegraphy
1910	J. D. van der Waals	Equation of state of gases and liquids
1911	W. Wien	Laws governing heat radiation
1912	N. G. Dalèn	Automatic regulators for lighting coastal beacons and light buoys

Et mei mollis scripta, et vim labores phaedrum, in cum facete saperet. Splendide elaboraret comprehensam qui ne. Putant verterem no vim, mea solum veritus definitiones ei, no labitur propriae deseruisse est. Ius illud everti salutandi id, eu facer pericula principes est.

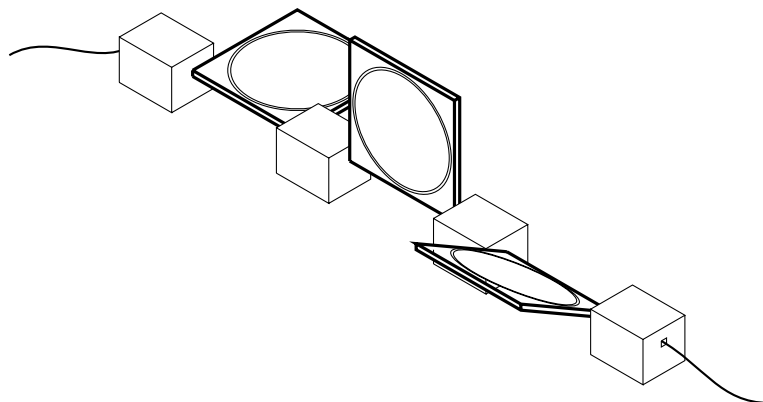


**Figure 3.2:** Fibre optics

Simul noster voluptaria eam ei, sint regione pri ei. Cum no utinam equidem, falli bonorum prodesset an qui. Alterum dissentiet vituperatoribus te eam, eos ea suas oblique. Per ea utinam facilisi. Docendi eligendi sit et, pri ea dicam eligendi percipitur, has soleat dolores convenire te.

Adipisci molestiae vim at, eum everti accommodare eu. Duo ex maiorum consetur. Sea et vivendo concludaturque, rebum conclusionemque pro eu. Mei an everti dolorem. Per id alterum mandamus deseruisse. Copiosae evertitur eum ea, atqui interesset est in. Vim magna munere nostrum an, cu congrue equidem est. Mediocre reformidans ne mel. Et summo nihil mel, an nam postea incorrupte.

In amet verear evertitur qui, ex mea vivendo hendrerit. Ad posse perfecto prodesset usu, cum fugit accumsan no. Tempor nonumes duo ea, oblique fabulas salutatus ne vis. Ne eam scripta dolorem, graece eruditi eum ei. Ei sed brute zril nostro, nostro voluptatum id sea, courtesy of Wikipedia. [81] Adipisci molestiae vim at, eum everti accommodare eu. Duo ex maiorum consetetur. Sea et vivendo concludaturque, rebum conclusionemque pro eu.

Adipisci molestiae vim at, eum everti accommodare eu. Duo ex maiorum consetetur. Sea et vivendo concludaturque, rebum conclusionemque pro eu. Mei an everti dolorem. Per id alterum mandamus deseruisse. Copiosae evertitur eum ea, atqui interesset est in. Vim magna munere nostrum an, cu congrue equidem est. Mediocre reformidans ne mel. Et summo nihil mel, an nam postea incorrupte an everti dolorem. Per id alterum mandamus deseruisse. Copiosae evertitur eum ea, atqui interesset est in. Vim magna munere nostrum an, cu congrue equidem est. Mediocre reformidans ne mel. Et summo nihil mel, an nam postea incorrupte. Mediocre reformidans ne mel. Et summo nihil mel, an nam postea incorrupte an everti dolorem.

Per id alterum mandamus deseruisse. Copiosae evertitur eum ea, atqui interesset est in. Vim magna munere nostrum an, cu congrue equidem est. Mediocre reformidans ne mel. Et summo nihil mel, an nam postea incorrupte.

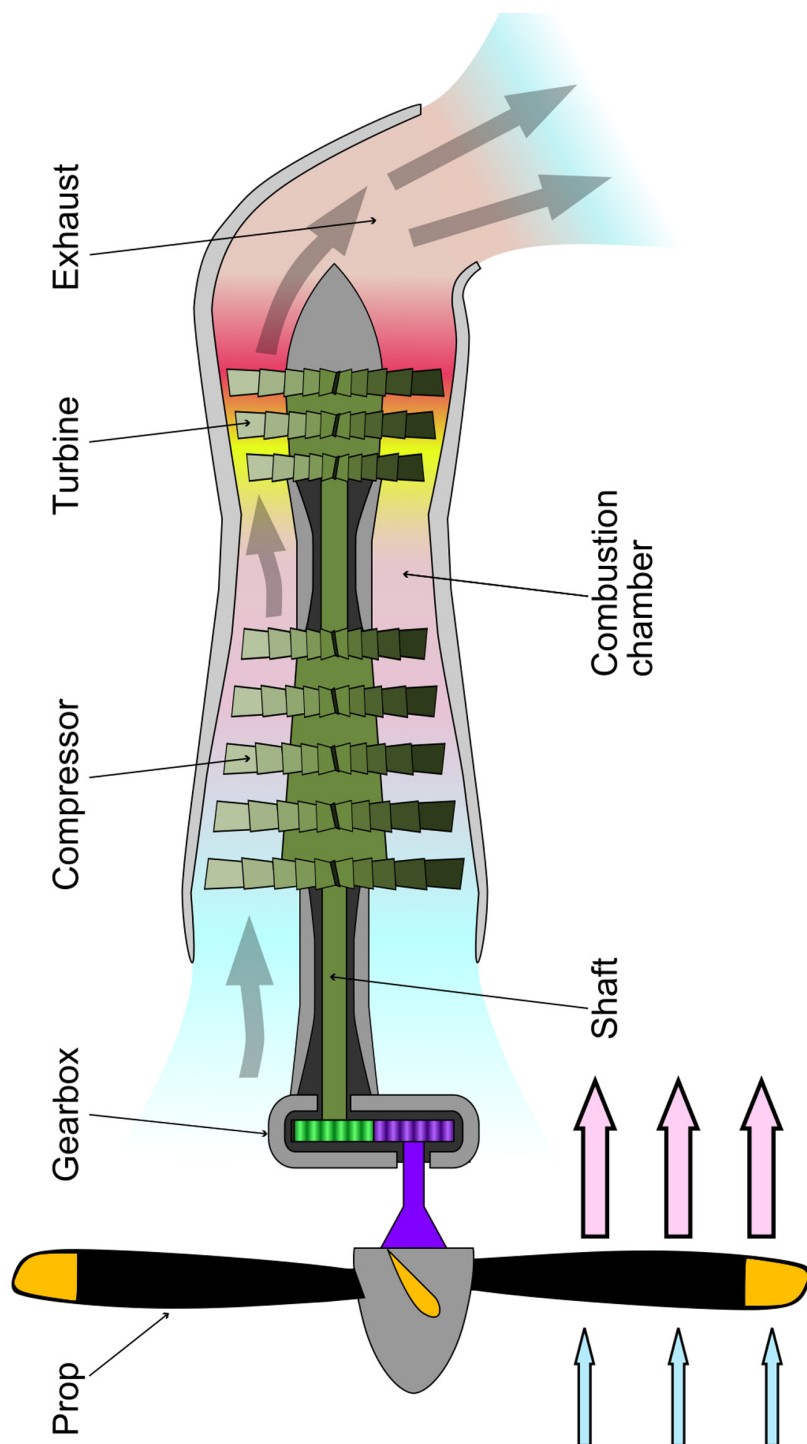


**Figure 3.3:** A landscape view of a Turboprop engine - these are jet engine derivatives, still gas turbines, that extract work from the hot-exhaust jet to turn a rotating shaft, which is then used to produce thrust by some other means



Id ius soluta semper audiam, ad eos scriptorem concludaturque, id mel rebum volumus deserunt. Mel libris percipit scriptorem te, his an dicat putent menandri, mazim officiis aliquando mei no. Ne clita veniam disputando vim, postea hendrerit maiestatis qui id. Mei te suscipit quaerendum, an aliquando intellegebat ius, ei simul detraxit dissentiet eam. Zril dolor ut usu.

Everti saperet vis ut. Scripta malisset mel eu, duis antiopam in pro. Sea diceret contentiones ea. Nec eu duis efficiantur, evertitur constituam mediocritatem te vis, pro error regione ad. Sit malorum aliquam at, pericula dissentias mei ei. Cu soluta urbanitas est, albucius vituperatoribus usu et.



# References

- [1] ABBOUD, T., RUSTOM, J., BESTER, M., CZORLICH, P., VITTORAZZI, E., PINNSCHMIDT, H. O., WESTPHAL, M., AND REGELSBERGER, J. Morphology of ruptured and unruptured intracranial aneurysms. *World neurosurgery* 99 (2017), 610–617.
- [2] AIRD, W. Spatial and temporal dynamics of the endothelium. *Journal of Thrombosis and Haemostasis* 3, 7 (2005), 1392–1406.
- [3] AL-SOUDI, A., KAAIJ, M., AND TAS, S. Endothelial cells: From innocent bystanders to active participants in immune responses. *Autoimmunity Reviews* 16, 9 (2017), 951 – 962.
- [4] ANDERSON, E., BAI, Z., BISCHOF, C., BLACKFORD, S., DEMMEL, J., DONGARRA, J. J., CROZ, J. D., GREENBAUM, A., HAMMARLING, S., MCKENNEY, A., AND SORENSEN, D. *LAPACK Users’ Guide*, 3 ed. Society for Industrial and Applied Mathematics, Philadelphia, PA, 1999.

- [5] ANTIGA, L., AND STEINMAN, D. A. Robust and objective decomposition and mapping of bifurcating vessels. *IEEE transactions on medical imaging* 23, 6 (2004), 704–713.
- [6] AOKI, T., KATAOKA, H., MORIMOTO, M., NOZAKI, K., AND HASHIMOTO, N. Macrophage-derived matrix metalloproteinase-2 and -9 promote the progression of cerebral aneurysms in rats. *Stroke* 38, 162–169.
- [7] AOKI, T., YAMAMOTO, K., FUKUDA, M., SHIMOGONYA, Y., FUKUDA, S., AND NARUMIYA, S. Sustained expression of mcp-1 by low wall shear stress loading concomitant with turbulent flow on endothelial cells of intracranial aneurysm. *Acta Neuropathologica Communications* 4, 1 (2016), 48.
- [8] BACKES, D., RINKEL, G. J., LABAN, K. G., ALGRA, A., AND VERGOUWEN, M. D. Patient- and aneurysm-specific risk factors for intracranial aneurysm growth. *Stroke* 47, 4 (2016), 951–957.
- [9] BACKES, D., VERGOUWEN, M. D., VELTHUIS, B. K., VAN DER SCHAAF, I. C., BOR, A. S. E., ALGRA, A., AND RINKEL, G. J. Difference in aneurysm characteristics between ruptured and unruptured aneurysms in patients with multiple intracranial aneurysms. *Stroke* 45, 5 (2014), 1299–1303.
- [10] BAEK, H., JAYARAMAN, M., RICHARDSON, P., AND KARNIADAKIS, G. Flow instability and wall shear stress variation in intracranial aneurysms. *Journal of the Royal Society Interface* (2009), rsif20090476.

- [11] BALAGURU, U. M., SUNDARESAN, L., MANIVANNAN, J., MAJUNATHAN, R., MANI, K., SWAMINATHAN, A., VENKATESAN, S., KASIVISWANATHAN, D., AND CHATTERJEE, S. Disturbed flow mediated modulation of shear forces on endothelial plane: A proposed model for studying endothelium around atherosclerotic plaques. *Scientific reports* 6 (2016), 27304.
- [12] BARATCHI, S., KHOSHMANESH, K., WOODMAN, O. L., POTOCHNIK, S., PETER, K., AND MCINTYRE, P. Molecular sensors of blood flow in endothelial cells. *Trends in molecular medicine* 23, 9 (2017), 850–868.
- [13] BARÁTH, K., CASSOT, F., RÜFENACHT, D. A., AND FASEL, J. H. Anatomically shaped internal carotid artery aneurysm in vitro model for flow analysis to evaluate stent effect. *American Journal of Neuroradiology* 25, 10 (2004), 1750–1759.
- [14] BAZILEVS, Y., HSU, M.-C., ZHANG, Y., WANG, W., KVAMSDAL, T., HENTSCHEL, S., AND ISAKSEN, J. Computational vascular fluid–structure interaction: methodology and application to cerebral aneurysms. *Biomechanics and modeling in mechanobiology* 9, 4 (2010), 481–498.
- [15] BENNDORF, G., WELLNHOFER, E., LANKSCH, W., AND FELIX, R. Intraaneurysmal flow: evaluation with doppler guidewires. *American journal of neuroradiology* 17, 7 (1996), 1333–1337.

- [16] BIASETTI, J., HUSSAIN, F., AND GASSER, T. C. Blood flow and coherent vortices in the normal and aneurysmatic aortas: a fluid dynamical approach to intra-luminal thrombus formation. *Journal of The Royal Society Interface* (2011), rsif20110041.
- [17] BOUSSEL, L., RAYZ, V., MCCULLOCH, C., MARTIN, A., ACEVEDO-BOLTON, G., LAWTON, M., HIGASHIDA, R., SMITH, W. S., YOUNG, W. L., AND SALONER, D. Aneurysm growth occurs at region of low wall shear stress: patient-specific correlation of hemodynamics and growth in a longitudinal study. *Stroke* 39, 11 (2008), 2997–3002.
- [18] BRINJIKJI, W., ZHU, Y.-Q., LANZINO, G., CLOFT, H., MURAD, M., WANG, Z., AND KALLMES, D. Risk factors for growth of intracranial aneurysms: A systematic review and meta-analysis. *American Journal of Neuroradiology* (2015).
- [19] BRISMAN, J. L., SONG, J. K., AND NEWELL, D. W. Cerebral aneurysms. *New England journal of medicine* 355, 9 (2006), 928–939.
- [20] BYRNE, G., AND CEBRAL, J. Vortex dynamics in cerebral aneurysms. *arXiv preprint arXiv:1309.7875* (2013).
- [21] BYRNE, G., MUT, F., AND CEBRAL, J. Quantifying the large-scale hemodynamics of intracranial aneurysms. *American Journal of Neuroradiology* 35, 2 (2014), 333–338.

- [22] CAN, A., AND DU, R. Association of hemodynamic factors with intracranial aneurysm formation and rupture: systematic review and meta-analysis. *Neurosurgery* 78, 4 (2015), 510–520.
- [23] CAR, R., AND PARRINELLO, M. Unified Approach for Molecular Dynamics and Density-Functional Theory. *Physical Review Letters* 55 (1985), 2471.
- [24] CASTRO, M. A., OLIVARES, M. C. A., PUTMAN, C. M., AND CEBRAL, J. R. Wall motion and hemodynamics in intracranial aneurysms. In *Journal of Physics: Conference Series* (2013), vol. 477, IOP Publishing, p. 012004.
- [25] CEBRAL, J., OLLIKAINEN, E., CHUNG, B. J., MUT, F., SIPPOLA, V., JAHROMI, B. R., TULAMO, R., HERNESNIEMI, J., NIEMELÄ, M., ROBERTSON, A., AND FRÖSEN, J. Flow conditions in the intracranial aneurysm lumen are associated with inflammation and degenerative changes of the aneurysm wall. *American Journal of Neuroradiology* 38, 1 (2017), 119–126.
- [26] CEBRAL, J. R., MUT, F., WEIR, J., AND PUTMAN, C. M. Association of hemodynamic characteristics and cerebral aneurysm rupture. *American Journal of Neuroradiology* 32, 2 (2011), 264–270.
- [27] CECCHI, E., GIGLIOLI, C., VALENTE, S., LAZZERI, C., GENSINI, G. F., ABBATE, R., AND MANNINI, L. Role of hemodynamic shear stress in cardiovascular disease. *Atherosclerosis* 214, 2 (2011), 249–256.

- [28] CHALOUHI, N., ALI, M. S., JABBOUR, P. M., TJOUMAKARIS, S. I., GONZALEZ, L. F., ROSENWASSER, R. H., KOCH, W. J., AND DUMONT, A. S. Biology of intracranial aneurysms: role of inflammation. *Journal of Cerebral Blood Flow & Metabolism* 32, 9 (2012), 1659–1676.
- [29] CHALOUHI, N., HOH, B. L., AND HASAN, D. Review of cerebral aneurysm formation, growth, and rupture. *Stroke* 44, 12 (2013), 3613–3622.
- [30] CHALOUHI, N., ZANATY, M., WHITING, A., YANG, S., TJOUMAKARIS, S., HASAN, D., STARKE, R. M., HANN, S., HAMMER, C., KUNG, D., AND ET. AL. Safety and efficacy of the pipeline embolization device in 100 small intracranial aneurysms. *Journal of neurosurgery* 122, 6 (2015), 1498–1502.
- [31] CHEN, C.-N., CHANG, S.-F., LEE, P.-L., CHANG, K., CHEN, L.-J., USAMI, S., CHIEN, S., AND CHIU, J.-J. Neutrophils, lymphocytes, and monocytes exhibit diverse behaviors in transendothelial and subendothelial migrations under coculture with smooth muscle cells in disturbed flow. *Blood* 107, 5 (2006), 1933–1942.
- [32] CHEN, Z., AND TZIMA, E. Pecam-1 is necessary for flow-induced vascular remodeling. *Arteriosclerosis, thrombosis, and vascular biology* 29, 7 (2009), 1067–1073.



- [33] CHIEN, S. Mechanotransduction and endothelial cell homeostasis: the wisdom of the cell. *American Journal of Physiology-Heart and Circulatory Physiology* 292, 3 (2007), H1209–H1224.
- [34] CHIU, J.-J., AND CHIEN, S. Effects of disturbed flow on vascular endothelium: pathophysiological basis and clinical perspectives. *Physiological reviews* 91, 1 (2011), 327–387.
- [35] CORNELISSEN, B., SCHNEIDERS, J., POTTERS, W., VAN DEN BERG, R., VELTHUIS, B., RINKEL, G., SLUMP, C., VANBAVEL, E., MAJOIE, C., AND MARQUERING, H. Hemodynamic differences in intracranial aneurysms before and after rupture. *American Journal of Neuroradiology* 36, 10 (2015), 1927–1933.
- [36] THE CPMD CONSORTIUM. *CPMD (v3.15.1): An ab initio Electronic Structure and Molecular Dynamics Program*, 2011.
- [37] DELLEY, B. An All-Electron Numerical Method for Solving the Local Density Functional for Polyatomic Molecules. *Journal of Chemical Physics* 92 (1990), 508.
- [38] DELLEY, B. Fast Calculation of Electrostatics in Crystals and Large Molecules. *Journal of Physical Chemistry* 100 (1996), 6107.
- [39] DEMARTINI, L. C., VIELMO, H. A., AND MÖLLER, S. Numeric and experimental analysis of the turbulent flow through a channel with baffle plates.

*Journal of the Brazilian Society of Mechanical Sciences and Engineering* 26, 2 (2004), 153–159.

- [40] DEMPÈRE-MARCO, L., OUBEL, E., CASTRO, M., PUTMAN, C., FRANGI, A., AND CEBRAL, J. Cfd analysis incorporating the influence of wall motion: application to intracranial aneurysms. In *International Conference on Medical Image Computing and Computer-Assisted Intervention* (2006), Springer, pp. 438–445.
- [41] DEPLANO, V., KNAPP, Y., BERTRAND, E., AND GAILLARD, E. Flow behaviour in an asymmetric compliant experimental model for abdominal aortic aneurysm. *Journal of biomechanics* 40, 11 (2007), 2406–2413.
- [42] DIAGBOUGA, M. R., MOREL, S., BIJLENGA, P., AND KWAK, B. R. Role of hemodynamics in initiation/growth of intracranial aneurysms. *European journal of clinical investigation* 48, 9 (2018), e12992.
- [43] DOLAN, J. M., KOLEGA, J., AND MENG, H. High wall shear stress and spatial gradients in vascular pathology: a review. *Annals of biomedical engineering* 41, 7 (2013), 1411–1427.
- [44] DOLAN, J. M., MENG, H., SINGH, S., PALUCH, R., AND KOLEGA, J. High fluid shear stress and spatial shear stress gradients affect endothelial proliferation, survival, and alignment. *Annals of biomedical engineering* 39, 6 (2011), 1620–1631.

- [45] DONGARRA, J. J. LINPACK Working Note 3: Fortran BLAS Timing. *Argonne National Laboratory Report, ANL-80-24* (1980).
- [46] DONGARRA, J. J., BUNCH, J., MOLER, C., AND STEWART, G. W. *LINPACK User's Guide*. Society for Industrial and Applied Mathematics, Philadelphia, PA, 1979.
- [47] DONGARRA, J. J., CROZ, J. D., HAMMARLING, S., AND DUFF, I. S. A Set of Level 3 Basic Linear Algebra Subprograms. *Association for Computing Machinery Transactions on Mathematical Software* 16 (1990), 1.
- [48] DONGARRA, J. J., CROZ, J. D., HAMMARLING, S., AND HANSON, R. An Extended Set of FORTRAN Basic Linear Algebra Subprograms. *Association for Computing Machinery Transactions on Mathematical Software* 14 (1988), 1.
- [49] DOVESI, R., ORLANDO, R., CIVALLERI, B., ROETTI, C., SAUNDERS, V. R., AND ZICOVICH-WILSON, C. M. CRYSTAL: A Computational Tool for the Ab Initio Study of the Electronic Properties of Crystals. *Zeitschrift für Kristallographie* 220 (2005), 571.
- [50] DOVESI, R., SAUNDERS, V. R., ROETTI, C., ORLANDO, R., ZICOVICH-WILSON, C. M., PASCALE, F., CIVALLERI, B., DOLL, K., HARRISON, N. M., BUSH, I. J., D'ARCO, P., AND LLUNELL, M. *CRYSTAL 09 User's Manual*. University of Torino, Italy, 2009.

- [51] DUAN, Z., LI, Y., GUAN, S., MA, C., HAN, Y., REN, X., WE, L., LI, W., LO, J., AND YANG, Z. Morphological parameters and anatomical locations associated with rupture status of small intracranial aneurysms. *Scientific reports* 8 (2018).
- [52] EFRON, B., HASTIE, T., JOHNSTONE, I., TIBSHIRANI, R., AND ET. AL. Least angle regression. *The Annals of statistics* 32, 2 (2004), 407–499.
- [53] ELAD, D., AND EINAV, S. Physical and flow properties of blood. *Standard handbook of biomedical engineering and design* (2004), 3–1.
- [54] ENZMANN, D. R., ROSS, M. R., MARKS, M. P., AND PELC, N. J. Blood flow in major cerebral arteries measured by phase-contrast cine mr. *American journal of neuroradiology* 15, 1 (1994), 123–129.
- [55] ETMINAN, N., BROWN, R. D., BESEOGLU, K., JUVELA, S., RAYMOND, J., MORITA, A., TORNER, J. C., DERDEYN, C. P., RAABE, A., MOCCO, J., AND ET. AL. The unruptured intracranial aneurysm treatment score a multidisciplinary consensus. *Neurology* 85, 10 (2015), 881–889.
- [56] FALGOUT, R. D., AND YANG, U. M. HYPRE: A Library of High Performance Preconditioners. In *Proceedings of the International Conference on Computational Science - Part III* (London, UK, 2002), ICCS '02, Springer-Verlag, p. 632.
- [57] FELICIANI, G., POTTERS, W. V., VAN OOIJ, P., SCHNEIDERS, J. J., NEDERVEEN, A. J., VAN BAVEL, E., MAJOIE, C. B., AND MARQUERING, H. A.

- Multiscale 3-d+ t intracranial aneurysmal flow vortex detection. *IEEE Trans. Biomed. Engineering* 62, 5 (2015), 1355–1362.
- [58] FINCH, H. A comparison of methods for group prediction with high dimensional data. *Journal of Modern Applied Statistical Methods* 13, 2 (2014), 5.
- [59] FORD, M., HOI, Y., PICCINELLI, M., ANTIGA, L., AND STEINMAN, D. An objective approach to digital removal of saccular aneurysms: technique and applications. *The British Journal of Radiology* 82, special\_issue\_1 (2009), S55–S61.
- [60] FORD, M. D., ALPERIN, N., LEE, S. H., HOLDSWORTH, D. W., AND STEINMAN, D. A. Characterization of volumetric flow rate waveforms in the normal internal carotid and vertebral arteries. *Physiological measurement* 26, 4 (2005), 477.
- [61] FORD, M. D., NIKOLOV, H. N., MILNER, J. S., LOWNIE, S. P., DEMONT, E. M., KALATA, W., LOTH, F., HOLDSWORTH, D. W., AND STEINMAN, D. A. Piv-measured versus cfd-predicted flow dynamics in anatomically realistic cerebral aneurysm models. *Journal of biomechanical engineering* 130, 2 (2008), 021015.
- [62] FRIGO, M., AND JOHNSON, S. G. The Design and Implementation of FFTW3. In *Proceedings of the IEEE* (2005), vol. 93, p. 216.

- [63] FUNG, J. C. H. Residence time of inertial particles in a vortex. *Journal of Geophysical Research: Oceans* 105, C6 (2000), 14261–14272.
- [64] GABRIEL, S. A., DING, Y., AND FENG, Y. Quantifying the influence of oscillatory flow disturbances on blood flow. *Journal of Theoretical Biology* 430 (2017), 195 – 206.
- [65] GALE, J. D. Empirical Potential Derivation for Ionic Materials. *Philosophical Magazine B* 73 (1996), 3.
- [66] GALE, J. D. GULP - A Computer Program for the Symmetry Adapted Simulation of Solids. *Journal of Chemical Society, Faraday Transactions* 93 (1997), 629.
- [67] GREVING, J. P., WERMER, M. J., JR, M. J. B., MORIT, A., JUVELA, S., YONEKURA, M., ISHIBASHI, T., TORNER, J. C., NAKAYAMA, T., RINKEL, G. J., AND ET. AL. Development of the phases score for prediction of risk of rupture of intracranial aneurysms: a pooled analysis of six prospective cohort studies. *The Lancet Neurology* 13, 1 (2014), 59–66.
- [68] GSAM KIM, Y., PAR, Y., AND LIM, S. 3d simulations of blood flow dynamics in compliant vessels: normal, aneurysmal, and stenotic arteries. *Communications in Computational Physics* 19, 5 (2016), 1167–1190.
- [69] GWILLIAM, M. N., HOGGARD, N., CAPENER, D., SINGH, P., MARZO, A., VERMA, P. K., AND WILKINSON, I. D. Mr derived volumetric flow

- rate waveforms at locations within the common carotid, internal carotid, and basilar arteries. *Journal of Cerebral Blood Flow & Metabolism* 29, 12 (2009), 1975–1982.
- [70] HACKENBERG, K. A., HÄNGGI, D., AND ETMINAN, N. Unruptured intracranial aneurysms: Contemporary data and management. *Stroke* 49, 9 (2018), 2268–2275.
- [71] HAIMES, R., AND KENWRIGHT, D. On the velocity gradient tensor and fluid feature extraction. In *14th Computational Fluid Dynamics Conference* (1999), p. 3288.
- [72] HANCZAR, B., HU, J., SIM, C., WEINSTEIN, J., BITTNER, M., AND RDOUGHERTY, E. Small-sample precision of roc-related estimates. *Bioinformatics* 26, 6 (2010), 822–830.
- [73] HANLEY, J. A., AND MCNEIL, B. J. The meaning and use of the area under a receiver operating characteristic (roc) curve. *Radiology* 143, 1 (1982), 29–36.
- [74] HARRELL, F. E., LEE, K. L., AND MARK, D. B. Multivariable prognostic models: issues in developing models, evaluating assumptions and adequacy, and measuring and reducing errors. *Statistics in medicine* 15, 4 (1996), 361–387.
- [75] HASAN, D. M., NADAREYSHVILI, A. I., HOPPE, A. L., MAHANE, K. B., KUNG, D. K., AND RAGHAVAN, M. L. Cerebral aneurysm sac growth as the

- etiology of recurrence after successful coil embolization. *Stroke* 43, 3 (2012), 866–868.
- [76] HASHIMOTO, T., MENG, H., AND YOUNG, W. Intracranial aneurysms: links among inflammation, hemodynamics and vascular remodeling. *Neurol Res* 28 (2006), 372–380.
- [77] HELMKE, B. P. Molecular control of cytoskeletal mechanics by hemodynamic forces. *Physiology* 20, 1 (2005), 43–53.
- [78] HESS, B., KUTZNER, C., VAN DER SPOEL, D., AND LINDAHL, E. GROMACS 4: Algorithms for Highly Efficient, Load-Balanced, and Scalable Molecular Simulation. *Journal of Chemical Theory and Computation* 4 (2008), 235.
- [79] HOLDSWORTH, D., NORLEY, C., FRAYNE, R., STEINMAN, D., AND RUTT, B. Characterization of common carotid artery blood-flow waveforms in normal human subjects. *Physiological measurement* 20, 3 (1999), 219.
- [80] HOPPE, A. L., RAGHAVA, M. L., AND HASAN, D. M. Comparison of the association of sac growth and coil compaction with recurrence in coil embolized cerebral aneurysms. *PloS one* 10, 4 (2015), e0123017.
- [81] [HTTP://WIKIPEDIA.ORG/](http://WIKIPEDIA.ORG/). *Wikipedia*. Wikipedia, The Internet, 2012.
- [82] HUGHES, J. D., BOND, K. M., MEKARY, R. A., DEWAN, M. C., RATTANI, A., BATICULON, R., KATO, Y., AZEVEDO-FILHO, H., MORCOS, J. J., AND



- PARK, K. B. Estimating the global incidence of aneurysmal subarachnoid hemorrhage: a systematic review for central nervous system vascular lesions and meta-analysis of ruptured aneurysms. *World neurosurgery* 115 (2018), 430–447.
- [83] HUMPHREY, W., DALKE, A., AND SCHULTEN, K. VMD - Visual Molecular Dynamics. *Journal of Molecular Graphics* 14 (1996), 33.
- [84] HUNT, J. C., WRAY, A. A., AND MOIN, P. Eddies, streams, and convergence zones in turbulent flows.
- [85] HUO, Y., CHOY, J. S., SVENDSEN, M., SINHA, A. K., AND KASSAB, G. S. Effects of vessel compliance on flow pattern in porcine epicardial right coronary arterial tree. *Journal of biomechanics* 42, 5 (2009), 594–602.
- [86] ILDIKO, F. E., AND FRIEDMAN, J. H. A statistical view of some chemometrics regression tools. *Technometrics* 35, 2 (1993), 109–135.
- [87] INVESTIGATORS, U. J. The natural course of unruptured cerebral aneurysms in a japanese cohort. *New England Journal of Medicine* 366, 26 (2012), 2474–2482.
- [88] JEONG, J., AND HUSSAIN, F. On the identification of a vortex. *Journal of fluid mechanics* 285 (1995), 69–94.
- [89] JIANG, J., AND STROTHER, C. M. Interactive decomposition and mapping of saccular cerebral aneurysms using harmonic functions: its first application

- with patient-specific computational fluid dynamics (cfd) simulations. *IEEE transactions on medical imaging* 32, 2 (2013), 153–164.
- [90] JIANG, M., MACHIRAJU, R., AND THOMPSON, D. Detection and visualization of vortices. *The visualization handbook* 295 (2005).
- [91] JR, M. A. G., AND GARCÍA-CARDEÑA, G. Endothelial cell dysfunction and the pathobiology of atherosclerosis. *Circulation research* 118, 4 (2016), 620–636.
- [92] JR, T. R. F., BENITEZ, R., VEZNEDAROGLU, E., SHARAN, A., MITCHELL, W., SILVA, M., AND ROSENWASSER, R. H. A review of size and location of ruptured intracranial aneurysms. *Neurosurgery* 49, 6 (2001), 1322–1326.
- [93] JUVELA, S. Risk factors for multiple intracranial aneurysms. *Stroke* 31, 2 (2000), 392–397.
- [94] JUVELA, S., POUSSA, K., LEHTO, H., AND PORRAS, M. Natural history of unruptured intracranial aneurysms: a long-term follow-up study. *Stroke* 44, 9 (2013), 2414–2421.
- [95] KARINO, T., AND GOLDSMITH, H. Flow behaviour of blood cells and rigid spheres in an annular vortex. *Phil. Trans. R. Soc. Lond. B* 279, 967 (1977), 413–445.
- [96] KASHIWAZAKI, D., AND KURODA, S. Size ratio can highly predict rupture risk in intracranial small ( $\leq 5$  mm) aneurysms. *Stroke* 44, 8 (2013), 2169–2173.

- [97] KAUFMANN, B. A., SANDERS, J. M., DAVIS, C., XIE, A., ALDRED, P., SAREMBOCK, I. J., AND LIDNER, J. R. Molecular imaging of inflammation in atherosclerosis with targeted ultrasound detection of vascular cell adhesion molecule-1. *Circulation* 116, 3 (2007), 276–284.
- [98] KHAN, M., VALEN-SENDSTAD, K., AND STEINMAN, D. Narrowing the expertise gap for predicting intracranial aneurysm hemodynamics: impact of solver numerics versus mesh and time-step resolution. *American Journal of Neuroradiology* (2015).
- [99] KIM, M.-C., NAM, J. H., AND LEE, C.-S. Near-wall deposition probability of blood elements as a new hemodynamic wall parameter. *Annals of Biomedical Engineering* 34, 6 (Jun 2006), 958–970.
- [100] KÖHLER, B., GASTEIGER, R., PREIM, U., THEISEL, H., GUTBERLET, M., AND PREIM, B. Semi-automatic vortex extraction in 4d pc-mri cardiac blood flow data using line predicates. *IEEE Transactions on Visualization and Computer Graphics* 19, 12 (2013), 2773–2782.
- [101] KOLÁŘ, V. Vortex identification: New requirements and limitations. *International journal of heat and fluid flow* 28, 4 (2007), 638–652.
- [102] KOLKAJI, A. *Molecular Graphics Modelling* 17 (1999), 176.
- [103] KOMOTAR, R. J., MOCCO, J., AND SOLOMON, R. A. Guidelines for the surgical treatment of unruptured intracranial aneurysms: the first annual j.

- lawrence pool memorial research symposium controversies in the management of cerebral aneurysms. *Neurosurgery* 62, 1 (2008), 183–194.
- [104] KORJA, M., LEHTO, H., AND JUVELA, S. Lifelong rupture risk of intracranial aneurysms depends on risk factors. *Stroke* 45, 7 (2014), 1958–1963.
- [105] KOSIERKIEWICZ, T., FACTOR, S., AND DICKSON, D. Immunocytochemical studies of atherosclerotic lesions of cerebral berry aneurysms. *J Neuropathol Exp Neurol* 53, 4 (1994), 399–406.
- [106] KOTOWSKI, M., NAGGARA, O., DARSAUT, T. E., NOLET, S., GEVRY, G., KOUZNETSOV, E., AND RAYMOND, J. Safety and occlusion rates of surgical treatment of unruptured intracranial aneurysms: a systematic review and meta-analysis of the literature from 1990 to 2011. *Journal of Neurology, Neurosurgery & Psychiatry* 84, 1 (2013), 42–48.
- [107] KRESSE, G., AND HAFNER, J. Ab Initio Molecular Dynamics for Liquid Metals. *Physical Review B* 47 (1993), 558.
- [108] KRESSE, G., AND HAFNER, J. Ab Initio Molecular-Dynamics Simulation of the Liquid-Metal-Amorphous-Semiconductor Transition in Germanium. *Physical Review B* 49 (1994), 14251.
- [109] KU, D., GIDDEN, D., PHILLIPS, D., AND JR, D. S. Hemodynamics of the normal human carotid bifurcation: in vitro and in vivo studies. *Ultrasound in medicine & biology* 11, 1 (1985), 13–26.

- [110] KU, D., GIDDENS, D. P., ZARINS, C. K., AND GLAGOV, S. Pulsatile flow and atherosclerosis in the human carotid bifurcation. positive correlation between plaque location and low oscillating shear stress. *Arteriosclerosis: An Official Journal of the American Heart Association, Inc.* 5, 3 (1985), 293–302.
- [111] KULCSÁR, Z., UGRON, A., BERENTEI, Z., PAÁL, G., SZIKORA, I., AND ET AL. Hemodynamics of cerebral aneurysm initiation: the role of wall shear stress and spatial wall shear stress gradient. *American Journal of neuroradiology* (2011).
- [112] LEE, G., EOM, K., LEE, C., KIM, D., AND KANG, S. Rupture of very small intracranial aneurysms: Incidence and clinical characteristics. *J Cerebrovasc Endovasc Neurosurg* 17(3) (2015), 217–222.
- [113] LIU, J., JING, L., WANG, C., ZHANG, Y., AND YANG, X. Recanalization, regrowth, and delayed rupture of a previously coiled unruptured anterior communicating artery aneurysm: a longitudinal hemodynamic analysis. *World neurosurgery* 89 (2016), 726–e5.
- [114] LIU, X., SUN, A., FAN, Y., AND DENG, X. Physiological significance of helical flow in the arterial system and its potential clinical applications. *Annals of Biomedical Engineering* 43, 1 (Jan 2015), 3–15.
- [115] LONGO, M., GRANATA, F., RACCHIUSA, S., MORMINA, E., GRASSO, G., LONGO, G. M., GARUFI, G., SALPIETRO, F. M., AND ALAFACI, C. Role

- of hemodynamic forces in unruptured intracranial aneurysms: An overview of a complex scenario. *World Neurosurgery* 105 (2017), 632 – 642.
- [116] LORENSEN, W. E., AND CLINE, H. E. Marching cubes: A high resolution 3d surface construction algorithm. In *ACM siggraph computer graphics* (1987), vol. 21, ACM, pp. 163–169.
- [117] MA, D., TREMMEL, M., PALUCH, R. A., LEVY, E. L. I., MENG, H., AND MOCCO, J. Size ratio for clinical assessment of intracranial aneurysm rupture risk. *Neurological research* 32, 5 (2010), 482–486.
- [118] MA, J., WANG, C., SHENE, C.-K., AND JIANG, J. A graph-based interface for visualanalytics of 3d streamlines and pathlines. *IEEE transactions on visualization and computer graphics* 20, 8 (2014), 1127–1140.
- [119] MANNINO, R. G., MYERS, D. R., AHN, B., WANG, Y., ROLLINS, M., GOLE, H., LIN, A. S., GULDBERG, R. E., GIDDENS, D. P., TIMMINS, L. H., AND ET. AL. Do-it-yourself in vitro vasculature that recapitulates in vivo geometries for investigating endothelial-blood cell interactions. *Scientific reports* 5 (2015), 12401.
- [120] MARKL, M., WEGENT, F., ZECH, T., BAUER, S., STRECKER, C., SCHUMACHER, M., WEILLER, C., HENNIG, J., AND HARLOFF, A. In vivo wall shear stress distribution in the carotid artery: effect of bifurcation geometry,

- internal carotid artery stenosis, and recanalization therapy. *Circulation: Cardiovascular Imaging* 3, 6 (2010), 647–655.
- [121] MASCITELLI, J. R., OERMANN, E. K., LEACY, R. A. D., MOYLE, H., MOCCO, J., AND PATEL, A. B. Predictors of treatment failure following coil embolization of intracranial aneurysms. *Journal of Clinical Neuroscience* 22, 8 (2015), 1275–1281.
- [122] MECKEL, S., STALDER, A. F., SANTINI, F., RADÜ, E.-W., RÜFENACHT, D. A., MARKL, M., AND WETZEL, S. G. In vivo visualization and analysis of 3-d hemodynamics in cerebral aneurysms with flow-sensitized 4-d mr imaging at 3 t. *Neuroradiology* 50, 6 (2008), 473–484.
- [123] MENG, H., TUTINO, V. M., XIANG, J., AND SIDDIQUI, A. High wss or low wss? complex interactions of hemodynamics with intracranial aneurysm initiation, growth, and rupture: Toward a unifying hypothesis. *American Journal of Neuroradiology* 35, 7 (2014), 1254–1262.
- [124] MIURA, Y., ISHIDA, F., UMEDA, Y., TANEMURA, H., SUZUKI, H., MATSUSHIMA, S., SHIMOSAKA, S., AND TAKI, W. Low wall shear stress is independently associated with the rupture status of middle cerebral artery aneurysms. *Stroke* 44, 2 (2013), 519–521.
- [125] MOLYNEUX, A., KERR, R., GROUP, I. S. A. T. I. C., ET AL. International subarachnoid aneurysm trial (isat) of neurosurgical clipping versus endovascular

- coiling in 2143 patients with ruptured intracranial aneurysms: a randomized trial. *Journal of stroke and cerebrovascular diseases* 11, 6 (2002), 304–314.
- [126] NOBARI, S., MONGRAIN, R., LEASK, R., AND CARTIER, R. The effect of aortic wall and aortic leaflet stiffening on coronary hemodynamic: a fluid–structure interaction study. *Medical & biological engineering & computing* 51, 8 (2013), 923–936.
- [127] NOWICKI, K. W., HOSAKA, K., HE, Y., MCFETRIDGE, P. S., SCOTT, E. W., AND HOH, B. L. Novel high-throughput in vitro model for identifying hemodynamic-induced inflammatory mediators of cerebral aneurysm formation. *Hypertension* 64, 6 (2014), 1306–1313.
- [128] OELTZE-JAFRA, S., CEBRAL, J. R., JANIG, G., AND PREIM, B. Cluster analysis of vortical flow in simulations of cerebral aneurysm hemodynamics. *IEEE transactions on visualization and computer graphics* 22, 1 (2016), 757–766.
- [129] OLLIKAINEN, E., TULAMO, R., LEHTI, S., LEE-RUECKERT, M., HERNESNIEMI, J., NIEMEL, M., YL-HERTTUALA, S., KOVANEN, P. T., AND FRSEN, J. Smooth muscle cell foam cell formation, apolipoproteins, and abca1 in intracranial aneurysms: Implications for lipid accumulation as a promoter of aneurysm wall rupture. *Journal of Neuropathology and Experimental Neurology* 75, 7 (2016), 689–699.



- [130] ORDEJÓ, P., DRABOLD, D. A., GRUMBACH, M. P., AND MARTIN, R. M. Unconstrained Minimization Approach for Electronic Computations That Scales Linearly with System Size. *Physical Review B* 48 (1993), 14646.
- [131] OTANI, T., NAKAMURA, M., FUJINAKA, T., HIRATA, M., KURODA, J., SHIBANO, K., AND WADA, S. Computational fluid dynamics of blood flow in coil-embolized aneurysms: effect of packing density on flow stagnation in an idealized geometry. *Medical & biological engineering & computing* 51, 8 (2013), 901–910.
- [132] OUBEL, E., CRAENE, M. D., PUTMAN, C. M., CEBRAL, J. R., AND FRANGI, A. F. Analysis of intracranial aneurysm wall motion and its effects on hemodynamic patterns. In *Medical Imaging 2007: Physiology, Function, and Structure from Medical Images* (2007), vol. 6511, International Society for Optics and Photonics, p. 65112A.
- [133] PAPAIOANNOU, T. G., AND STEFANADIS, C. Vascular wall shear stress: basic principles and methods. *Hellenic J Cardiol* 46, 1 (2005), 9–15.
- [134] PENN, D. L., WITTE, S. R., KOMOTAR, R. J., AND JR, E. S. C. The role of vascular remodeling and inflammation in the pathogenesis of intracranial aneurysms. *Journal of clinical neuroscience* 21, 1 (2014), 28–32.

- [135] PICCINELLI, M., STEINMAN, D. A., HOI, Y., TONG, F., VENEZIANI, A., AND ANTIGA, L. Automatic neck plane detection and 3d geometric characterization of aneurysmal sacs. *Annals of Biomedical Engineering* 40, 10 (2012), 2188–2211.
- [136] PLIMPTON, S. J. Fast Parallel Algorithms for Short-Range Molecular Dynamics. *Journal of Computational Physics* 117 (1995), 1.
- [137] POETHKE, J., SPULER, A., PETZ, C., HEGE, H.-C., GOUBERGRITS, L., AFFELD, K., AND KERTZSCHER, U. Cerebral aneurysm hemodynamics and a length of parent vessel. In *World Congress on Medical Physics and Biomedical Engineering, September 7-12, 2009, Munich, Germany* (2009), Springer, pp. 1608–1611.
- [138] POTTERS, W. V., MARQUERING, H. A., VANBAVEL, E., AND NEDERVEEN, A. J. Measuring wall shear stress using velocity-encoded mri. *Current Cardiovascular Imaging Reports* 7, 4 (2014), 9257.
- [139] QIU, J., ZHENG, Y., HU, J., LIAO, D., GREGERSEN, H., DENG, X., FAN, Y., AND WANG, G. Biomechanical regulation of vascular smooth muscle cell functions: from in vitro to in vivo understanding. *Journal of The Royal Society Interface* 11, 90 (2014), 20130852.

- [140] R DEVELOPMENT CORE TEAM. *R: A Language and Environment for Statistical Computing*. R Foundation for Statistical Computing, Vienna, Austria, 2011.
- [141] REVILLA-PACHECO, F., ESCALANTE-SEYFFERT, M. C., HERRADA-PINEDA, T., MANRIQUE-GUZMAN, S., PEREZ-ZUNIGA, I., RANGEL-SUAREZ, S., RUBALCAVA-ORTEGA, J., AND LOYO-VARELA, M. Prevalence of incidental clinoid segment saccular aneurysms. *World neurosurgery* 115 (2018), e244–e251.
- [142] RINNE, J., HERNESNIEMI, J., PURANEN, M., AND SAARI, T. Multiple intracranial aneurysms in a defined population: prospective angiographic and clinical study. *Neurosurgery* 35, 5 (1994), 803–808.
- [143] ROCHA, A. R. *Theoretical and Computational Aspects of Electronic Transport at the Nanoscale*. PhD thesis, University of Dublin, Trinity College, 2007.
- [144] RUNGGER, I., AND SANVITO, S. Algorithm for the Construction of Self-Energies for Electronic Transport Calculations Based on Singularity Elimination and Singular Value Decomposition. *Physical Review B* 78 (2008), 035407.
- [145] SAWYER, D. M., PACE, L. A., PASCALE, C. L., KUTCHIN, A. C., ONEILL, B. E., STARKE, R. M., AND DUMONT, A. S. Lymphocytes influence intracranial aneurysm formation and rupture: role of extracellular matrix remodeling

- and phenotypic modulation of vascular smooth muscle cells. *Journal of neuroinflammation* 13, 1 (2016), 185.
- [146] SCHAFHITZEL, T., VOLLRATH, J. E., GOIS, J. P., WEISKOPF, D., CASTELO, A., AND ERTL, T. Topology-preserving  $\lambda^2$ -based vortex core line detection for flow visualization. In *Computer Graphics Forum* (2008), vol. 27, Wiley Online Library, pp. 1023–1030.
- [147] SCHAFTENAAR, G., AND NOORDIK, J. H. *Journal of Computer-Aided Molecular Design* 14 (2000), 123.
- [148] SFORZA, D. M., PUTMAN, C. M., AND CEBRAL, J. R. Hemodynamics of cerebral aneurysms. *Annual review of fluid mechanics* 41 (2009), 91–107.
- [149] SHANNON, C. E. A mathematical theory of communication. *ACM SIGMOBILE Mobile Computing and Communications Review* 5, 1 (2001), 3–55.
- [150] SHOJIMA, M., OSHIMA, M., TAKAGI, K., TORII, R., HAYAKAWA, M., KATADA, K., MORITA, A., AND KIRINO, T. Magnitude and role of wall shear stress on cerebral aneurysm: computational fluid dynamic study of 20 middle cerebral artery aneurysms. *Stroke* 35, 11 (2004), 2500–2505.
- [151] SI, H., AND GÄRTNER, K. 3d boundary recovery by constrained delaunay tetrahedralization. *International Journal for Numerical Methods in Engineering* 85, 11 (2011), 1341–1364.

- [152] SIGNORELLI, F., SELA, S., GESUALDO, L., CHEVREL, S., TOLLET, F.,  
 PAILLER-MATTEI, C., TACCONI, L., TURJMAN, F., VACCA, A., AND  
 SCHUL, D. B. Hemodynamic stress, inflammation, and intracranial aneurysm  
 development and rupture: A systematic review. *World Neurosurgery* 115  
 (2018), 234 – 244.
  
- [153] SOLER, J. M., ARTACHO, E., GALE, J. D., GARCÍA, A., JUNQUERA, J.,  
 ORDEJÓN, P., AND SÁNCHEZ-PORTAL, D. The SIESTA Method for Ab Ini-  
 tio Order-N Materials Simulation. *Journal of Physics: Condensed Matter* 14  
 (2002), 2745.
  
- [154] STARKE, R. M., RAPER, D. M., DING, D., CHALOUHI, N., OWENS, G. K.,  
 HASAN, D. M., MEDEL, R., AND DUMONT, A. S. Tumor necrosis factor-  
 $\alpha$  modulates cerebral aneurysm formation and rupture. *Translational stroke*  
*research* 5, 2 (2014), 269–277.
  
- [155] STEINER, T., JUVELA, S., UNTERBERG, A., JUNG, C., FORSTING, M., AND  
 RINKEL, G. European stroke organization guidelines for the management of in-  
 tracranial aneurysms and subarachnoid haemorrhage. *Cerebrovascular diseases*  
*(Basel, Switzerland)* 35 (02 2013), 93–112.
  
- [156] STEINMAN, D. A. Image-based computational fluid dynamics modeling in  
 realistic arterial geometries. *Annals of biomedical engineering* 30, 4 (2002),  
 483–497.

- [157] STEINMAN, D. A., MILNER, J. S., NORLEY, C. J., LOWNIE, S. P., AND HOLDSWORTH, D. W. Image-based computational simulation of flow dynamics in a giant intracranial aneurysm. *American Journal of Neuroradiology* 24, 4 (2003), 559–566.
- [158] SUJUDI, D., AND HAIMES, R. Identification of swirling flow in 3-d vector fields. In *12th Computational Fluid Dynamics Conference* (1995), p. 1715.
- [159] SUNDERLAND, K., HAFFERMAN, C., CHINTALAPANI, G., AND JIANG, J. Vortex analysis of intra-aneurysmal flow in cerebral aneurysms. *Computational and Mathematical Methods in Medicine* 2016 (2016).
- [160] THOMAS, A., OU-YANG, H. D., LOWE-KRENTZ, L., MUZYKANTOV, V. R., AND LIU, Y. Biomimetic channel modeling local vascular dynamics of pro-inflammatory endothelial changes. *BiOMICROFLUIDICS* 10, 1 (2016), 014101.
- [161] THOMPSON, G. B., BROWN, R. D., AMIN-HANJANI, S., BRODERICK, J. P., COCKROFT, K. M., CONNOLLY, E. S., DUCKWILER, G. R., HARRIS, C. C., HOWARD, V. J., JOHNSTON, S. C. C., AND ET. AL. Guidelines for the management of patients with unruptured intracranial aneurysms: a guideline for healthcare professionals from the american heart association/american stroke association. *Stroke* (2015), STR–0000000000000070.
- [162] TIBSHIRANI, R. Regression shrinkage and selection via the lasso. *Journal of the Royal Statistical Society. Series B (Methodological)* (1996), 267–288.

- [163] TIBSHIRANI, R., HASTIE, T., NARASIMHAN, B., AND CHU, G. Diagnosis of multiple cancer types by shrunken centroids of gene expression. *Proceedings of the National Academy of Sciences* 99, 10 (2002), 6567–6572.
  
- [164] TRONIC, F., MALLAT, Z., LEHOUX, S., WASSEF, M., ESPOSITO, B., AND TEDGUI, A. Role of matrix metalloproteinases in blood flow-induced arterial enlargement: interaction with no. *Arterioscler Thromb Vasc Biol* 20, 12 (2000), E120–E126.
  
- [165] TURJMA, A. S., TURJMAN, F., AND EDELMAN, E. R. Role of fluid dynamics and inflammation in intracranial aneurysm formation. *Circulation* 129, 3 (2014), 373–382.
  
- [166] TZIMA, E., IRANI-TEHRANI, M., KIOSSES, W. B., DEJANA, E., SCHULTZ, D. A., ENGELHARDT, B., CAO, G., DELISSER, H., AND SCHWARTZ, M. A. A mechanosensory complex that mediates the endothelial cell response to fluid shear stress. *Nature* 437, 7057 (2005), 426.
  
- [167] UHANA FRÖSEN, TULAMO, R., PAETAU, A., LAAKSAMO, E., KORJA, M., LAAKSO, A., MIKANIELMÄ, AND HERNESNIEMI, J. Saccular intracranial aneurysm: pathology and mechanisms. *Acta Neuropathologica* 123, 6 (Jun 2012), 773–786.

- [168] UZARSKI, J. S., SCOTT, E. W., AND MCFETRIDGE, P. S. Adaptation of endothelial cells to physiologically-modeled, variable shear stress. *PloS one* 8, 2 (2013), e57004.
- [169] VALEN-SENDSTAD, K., AND STEINMAN, D. Mind the gap: impact of computational fluid dynamics solution strategy on prediction of intracranial aneurysm hemodynamics and rupture status indicators. *American Journal of Neuroradiology* (2013).
- [170] VANHOUTTE, P. M., SHIMOKAWA, H., TANG, E. H., AND FELETOU, M. Endothelial dysfunction and vascular disease. *Acta physiologica* 196, 2 (2009), 193–222.
- [171] VARBLE, N., TUTINO, V., YU, J., SONIG, A., SIDDIQUI, A., DAVIES, J., AND MENG, H. Shared and distinct rupture discriminants of small and large intracranial. *Stroke* 49 (2018), 856–864.
- [172] VERSTEEG, H., AND MALALASEKERA, W. An introduction to computational fluid dynamics: the finite volume method.
- [173] VILLABLANCA, J. P., DUCKWILE, G. R., JAHAN, R., TATESHIMA, S., MARTIN, N. A., FRAZEE, J., GONZALEZ, N. R., SAYRE, J., AND VINUELA, F. V. Natural history of asymptomatic unruptured cerebral aneurysms evaluated at ct angiography: growth and rupture incidence and correlation with epidemiologic risk factors. *Radiology* 269, 1 (2013), 258–265.



- [174] VLAK, M. H., ALGRA, A., BRANDENBURG, R., AND RINKEL, G. J. Prevalence of unruptured intracranial aneurysms, with emphasis on sex, age, comorbidity, country, and time period: a systematic review and meta-analysis. *The Lancet Neurology* 10, 7 (2011), 626–636.
- [175] WANG, C., BAKER, B. M., CHEN, C. S., AND SCHWARTZ, M. A. Endothelial cell sensing of flow directionsignificance. *Arteriosclerosis, thrombosis, and vascular biology* 33, 9 (2013), 2130–2136.
- [176] WATTON, P., SELIMOVIC, A., RABERGER, N. B., HUANG, P., HOLZAPFEL, G., AND VENTIKOS, Y. Modelling evolution and the evolving mechanical environment of saccular cerebral aneurysms. *Biomechanics and modeling in mechanobiology* 10, 1 (2011), 109–132.
- [177] WEIR, B. Unruptured intracranial aneurysms: a review. *Journal of neurosurgery* 96, 1 (2002), 3–42.
- [178] WEIR, B., DISNEY, L., AND KARRISON, T. Sizes of ruptured and unruptured aneurysms in relation to their sites and the ages of patients. *Journal of neurosurgery* 96, 1 (2002), 64–70.
- [179] WEN, J., DING, G., JIANG, W., WANG, Q., AND ZHENG, T. Numerical simulation of compliant artery bypass grafts using fluid–structure interaction framework. *Asaio Journal* 60, 5 (2014), 533–540.

- [180] WILLIAMS, L. N., AND BROWN, R. D. Management of unruptured intracranial aneurysms. *Neurology: Clinical Practice* 3, 2 (2013), 99–108.
- [181] WOLF, F., VOGT, F., SCHMITZ-RODE, T., JOCKENHOEVEL, S., AND MELA, P. Bioengineered vascular constructs as living models for in vitro cardiovascular research. *Drug discovery today* 21, 9 (2016), 1446–1455.
- [182] XIANG, J., NATARAJAN, S. K., TREMMEL, M., MA, D., MOCCO, J., HOPKINS, L. N., SIDDIQUI, A. H., LEVY, E. I., AND MENG, H. Hemodynamic–morphologic discriminants for intracranial aneurysm rupture. *Stroke* 42, 1 (2011), 144–152.
- [183] XIANG, J., NATARAJAN, S. K., TREMMEL, M., MA, D., MOCCO, J., HOPKINS, L. N., SIDDIQUI, A. H., LEVY, E. I., AND MENG, H. Hemodynamic–morphologic discriminants for intracranial aneurysm rupture. *Stroke* 42, 1 (2011), 144–152.
- [184] XIANG, J., SIDDIQUI, A., AND MENG, H. The effect of inlet waveforms on computational hemodynamics of patient-specific intracranial aneurysms. *Journal of biomechanics* 47, 16 (2014), 3882–3890.
- [185] XIONG, G., FIGUEROA, C. A., XIAO, N., AND TAYLOR, C. A. Simulation of blood flow in deformable vessels using subject-specific geometry and spatially varying wall properties. *International journal for numerical methods in biomedical engineering* 27, 7 (2011), 1000–1016.

- [186] XU, L., GU, L., AND LIU, H. Exploring potential association between flow instability and rupture in patients with matched-pairs of ruptured–unruptured intracranial aneurysms. *Biomedical engineering online* 15, 2 (2016), 166.
- [187] XU, L., LEE, T.-Y., AND SHEN, H.-W. An information-theoretic framework for flow visualization. *IEEE Transactions on Visualization and Computer Graphics* 16, 6 (2010), 1216–1224.
- [188] YASUDA, R., STROTHER, C. M., TAKI, W., SHINKI, K., ROYALTY, K., PULFER, K., AND KARMONIK, C. Aneurysm volume-to-ostium area ratio: a parameter useful for discriminating the rupture status of intracranial aneurysms. *Neurosurgery* 68, 2 (2011), 310–318.
- [189] ZHANG, Y., JING, L., ZHANG, Y., LIU, J., AND YANG, X. Low wall shear stress is associated with the rupture of intracranial aneurysm with known rupture point: case report and literature review. *BMC Neurol* 16 (2016).
- [190] ZHAO, M., AMIN-HANJANI, S., RULAND, S., CURCIO, A., OSTERGREN, L., AND CHARBEL, F. Regional cerebral blood flow using quantitative mr angiography. *American Journal of Neuroradiology* 28, 8 (2007), 1470–1473.
- [191] ZHOU, G., ZHU, Y., YIN, Y., SU, M., AND LI, M. Association of wall shear stress with intracranial aneurysm rupture: systematic review and meta-analysis. *Scientific reports* 7, 1 (2017), 5331.

- [192] ZOU, H., AND HASTIE, T. Regularization and variable selection via the elastic net. *J.R. Statist. Soc. B* (2005), 301–320.

# Appendix A

## Statistics

In this type of predictive modeling, there exists an input-output dataset  $(X,Y) \in X \times Y$  with an unknown probability distribution  $P$ . The goal of predictive modeling is to find a function  $f_n : X \rightarrow Y$ , that is determined using a training set  $(X_1, Y_1, \dots, (X_n, Y_n))$  of  $n$  random pairs distributed as  $(X,Y)$ . A desirable solution of  $f_n$  is one that, given a new data-point  $x \in X$ , the resultant  $f_n(x)$  is an accurate prediction of the true output  $y \in Y$ . This desired outcomes not only relies on the chosen function's predictive accuracy, but also of the selecting of relevant variables that are capable of achieving desired predictions. For desired models, it is often preferred to find the prediction function that achieves the desired accuracy while using the minimal amount of variables required: i.e a *parsimonious* model. Brute-force methods of testing all variable combinations becomes increasingly unviable, especially when the

number of variables in a dataset is larger than the number of  $n$  data points (cases) available for analysis: often refereed to the "large  $p$ , small  $n$  paradigm". One type of methodology to determine a desired model is through the use of sparsity-based regularization methods [86, 162, 163, 192]

## Section 1

Multiple logistic regression (MLR) analysis looks both to estimate the odds of a dichotomous outcome occurring, and to determine the impact of an individual variable (covariate) in relation to the other covariates in a model. The probability of an outcome occurring in MLR can be calculated as such:

$$\hat{p} = \frac{\exp(b_0 + b_1X_1 + b_2X_2 + \dots + b_pX_p)}{1 + \exp(b_0 + b_1X_1 + b_2X_2 + \dots + b_pX_p)} \quad (\text{A.1})$$

$\hat{p}$  being the probability of the desired outcome,  $X_1$  through  $X_p$  as the individual dependent variables applied to the model, and  $b_1$  to  $b_p$  being each variable's (respective) regression coefficients. To determine the expected log odds ratios of the model's variables, the *logit* function of the above equation can be calculated:

$$\begin{aligned}
\text{logit}[\hat{p}] &= \ln\left[\frac{\hat{p}}{1-\hat{p}}\right] \\
&= \ln\left[\frac{\frac{\exp(b_0+b_1X_1+b_2X_2+\dots+b_pX_p)}{1+\exp(b_0+b_1X_1+b_2X_2+\dots+b_pX_p)}}{1-\frac{\exp(b_0+b_1X_1+b_2X_2+\dots+b_pX_p)}{1+\exp(b_0+b_1X_1+b_2X_2+\dots+b_pX_p)}}\right] \\
&= \ln\left[\frac{\frac{\exp(b_0+b_1X_1+b_2X_2+\dots+b_pX_p)}{1+\exp(b_0+b_1X_1+b_2X_2+\dots+b_pX_p)}}{\frac{1}{1+\exp(b_0+b_1X_1+b_2X_2+\dots+b_pX_p)}}\right] \tag{A.2} \\
&= \ln[\exp(b_0 + b_1X_1 + b_2X_2 + \dots + b_pX_p)] \\
&= b_0 + b_1X_1 + b_2X_2 + \dots + b_pX_p
\end{aligned}$$

Taking the *logit* of the desired outcome's probability, transforms the occurrence of the event given Xs into a simplified linear function.

For each variable added to a regression model, the resultant  $R^2$  (coefficient of multiple determination) may increase, indicating an improved fit of the data. However applying a large number of variables to a predictive model may result in over-fitting without a significantly large dataset: large  $p$ , small  $n$  paradigm. In such an event, the  $R^2$  values, regression coefficients, and any statistical significance ( $p$ -values) determined may be misleading. To reduce the initial choices of variables in assessed predictive models, the correlation between variables were determined. The correlation of data can be determine by:

$$r_{jk} = \frac{s_{jk}}{s_j s_k} = \frac{\sum_{i=1}^n (x_{ij} - \bar{x}_j)(x_{ik} - \bar{x}_k)}{\sqrt{\sum_{i=1}^n (x_{ij} - \bar{x}_j)^2} \sqrt{\sum_{i=1}^n (x_{ik} - \bar{x}_k)^2}} \tag{A.3}$$

with  $r$  as the Pearson correlation coefficient between variables  $x_j$  and  $x_k$ ,  $n$  as the sample size, and  $\bar{x}$  is a variable sample mean. Correlations between the variables are often displayed via a correlation table:

$$R = \begin{bmatrix} 1 & r_{12} & r_{13} & \dots & r_{1p} \\ r_{21} & 1 & r_{23} & \dots & r_{2p} \\ r_{31} & r_{32} & 1 & \dots & r_{3p} \\ \vdots & \vdots & \vdots & \ddots & \vdots \\ r_{p1} & r_{p2} & r_{p3} & \dots & 1 \end{bmatrix}$$

Initial correlation analysis of all available geometric and hemodynamic variables was performed to eliminate highly correlated variables from analysis: i.e aneurysm volume and surface area are highly correlated so surface area was removed from analysis.

From the remaining variables, stepwise MLR was implemented to determine the parsimonious model. In stepwise regression, a linear regression is first performed for each variable  $X$  one at a time, and the variable with the highest  $R^2$  is kept for the model. Next, a multiple regression step is performed with the kept variable and each remaining variable. The variable with the largest increase in  $R^2$ , if the  $p$  value of the  $R^2$  is below a desired cutoff ( $<0.05$ ), is added to the model. The calculation of the  $p$  value of an increase in  $R^2$  resulting from the increasing of  $X$  variable(s) from  $a$  to



$b$  is as follows:

$$p_{ab} = \frac{(R_b^2 - R_a^2)/(b - a)}{(1 - R_b^2)/(n - b - 1)} \quad (\text{A.4})$$

with the total sample size  $n$ .

Each time a new variable is added to the model, the impact of removing any of the other variables (already added to the model) on outcomes is tested. The chosen (removed) variable is excluded from the model if it does not make  $R^2$  significantly worse. This process is continued till adding any new variables does not increase  $R^2$  and removing any  $X$  variables does not significantly decrease  $R^2$ .

In the event that all of the independent variables in the model are completely uncorrelated with each other, the interpretation of coefficients are as such:

$$OR = \exp(b_1)^z \quad (\text{A.5})$$

Where  $z$  is the number of unit changes for a variable  $X$ , and  $OR$  is the odds ratio resultant from said change. When the variables are not uncorrelated, the  $OR = \exp^z b_1$  is expressed as the change of unit  $z$  for a variable *adjusted in relation to the impacts of the other variables in the model*. This stresses the need to assess collinearity between variables prior to model assessment.

in Section ??.

## Section 2

Limitations may arise in applying multiple logistic regression analysis to data sets with a large number of variables in relation to the number of samples.

The Nearest Shrunken Centroid (NSC) method is a statistical classification methodology developed by Tibshirani et al.[163] as a means to improve predictions in high-dimensional data. Additionally, a 2014 study by Finch [58] compared a number of methods for statistical group prediction. The NSC method was found to be robust in terms of accuracy and identification of predictor variables over other methods when dealing with high-dimensional datasets. Initially developed for predictions within genetic data, NSC aims to shrink class (e.g. rupture status) centroids towards the *overall* centroid of the entire data-set after standardizing by the within-class deviation for each variable. This standardization of the resultant centroid gives higher impact to variables whose expression is more stable within samples of the same class. Due to the number of geometric and hemodynamic variables that may impact IA rupture, the NSC method was investigated as a useful methodology to help predict rupture potential within our data-set.

In our study,  $x_{ijk}$  represents the value of quantified variables  $i = 1, \dots, p$  in aneurysm  $j = 1, \dots, n_k$  of class  $k$ . The mean for variable  $i$  in each class  $k$  is calculated

$$\bar{x}_{ik} = \sum_{j=1}^{n_k} \frac{x_{ijk}}{n_k} \quad (\text{A.6})$$

and the *overall* mean for variable  $i$  is calculated.

$$\bar{x}_i = \sum_{k=1}^K \sum_{j=1}^{n_k} \frac{x_{ijk}}{n_k} \quad (\text{A.7})$$

A  $t$ -statistic value,  $d_{ik}$ , for each variable is calculated, comparing class  $k$  to the overall mean:

$$d_{ik} = \frac{\bar{x}_{ik} - \bar{x}_i}{m_k \cdot (s_i + s_0)} \quad (\text{A.8})$$

with

$$s_i^2 = \frac{1}{n - K} \sum_{k=1}^K \sum_{j=1}^{n_k} (x_{ijk} - \bar{x}_{ik})^2 \quad (\text{A.9})$$

and

$$m_k = \sqrt{1/n_k + 1/n}, \text{ where } n = \sum_{k=1}^K n_k \quad (\text{A.10})$$

The  $s_0$  in (A.8) is used as a *regularization parameter* to help protect from large  $d_{ik}$  values occurring from variables at low expression levels. The value of  $s_0$  is determined

as the median value of  $s_i$  over the set of variables.

With the inclusion of  $d_{ik}$ , the class centroid can be rewritten as:

$$\bar{x}_{ik} = \bar{x}_i + m_k(s_i + S_0)d_{ik} \quad (\text{A.11})$$

The NSC method shrinks each  $d_{ik}$  toward zero, creating a new value  $d'_{ik}$  which generates a new shrunken centroid value

$$\bar{x}'_{ik} = \bar{x}_i + m_k(s_i + s_0)d'_{ik} \quad (\text{A.12})$$

The value of shrinkage is determined through *soft thresholding*, where the absolute value of  $d_{ik}$  is reduced by  $\Delta$  and is given the value of 0 if the result is  $< 0$ , with

$$d'_{ik} = \text{sign}(d_{ik})(|d_{ik}| - \Delta)_+ \quad (\text{A.13})$$

This combination of shrinkage and *soft thresholding* can result in many 'noisy'  $\bar{x}_{ik}$  being close to the value of the overall mean  $\bar{x}_i$ . If  $\Delta$  shrinks  $d_{ik}$  to zero for all  $k$ , then the centroid for variable  $i$  is the same for all classes and is excluded from prediction analysis.

The value of  $\Delta$  is determined through cross-validation: fitting the model for many values of  $\Delta$  and determining the level of error per chosen  $\Delta$ . The  $\Delta$  resulting in the smallest error was chosen for our prediction.

## Section 3

Elastic Net Regularization (ENR) overcomes some of the limitations of the LASSO selection method, primarily being able to accurately handle data sets with a high number of variables in relation to the sample size [52, 162]. Additionally, the ENR method is able to handle data sets with groups of highly correlated variables.

ENR solves two optimization problems:

$$\begin{aligned} \tilde{\beta} = \arg \min_{\beta} & \sum_{i=1}^N (y_i - (X\beta)_i)^2 \\ \text{subject to} & \sum_{j=1}^p |\beta_j| \leq t_1 \text{ and } \sum_{j=1}^p \beta_j^2 \leq t_2 \end{aligned} \tag{A.14}$$

where a penalty is placed on the  $L_1$  norm ( $\sum_{j=1}^p |\beta_j|$ ) and the  $L_2$  norm ( $\sum_{j=1}^p \beta_j^2 \leq t_2$ ) of the regression coefficients. The purpose of these penalties are as follows:  $L_1$  performs variable selection by setting some coefficients to 0, and  $L_2$  works toward group selection by shrinking the coefficients of correlated variables toward each other. Re-writing equation A.14 in the Lagrangian form using two tuning parameters ( $\lambda_1$  and  $\lambda_2$ )

is as follows:

$$\tilde{\beta} = \arg \min_{\beta} \left( \sum_{i=1}^N (y_i - (X\beta)_i)^2 + \lambda_1 \sum_{j=1}^p |\beta_j| + \lambda_2 \sum_{j=1}^p \beta_j^2 \right) \quad (\text{A.15})$$

The choice of tuning parameter values is performed by analyzing an array of  $\lambda_2$  values (0, 0.01, 0.1, 1, 10, and 100). For each value in the array, the LARS-EN algorithm calculates the resultant  $\lambda_1$  value. The *lambda*<sub>1</sub> value that yields the smallest *k*-fold cross validation error, and its *lambda*<sub>2</sub> value used to generate it, are used as the tuning parameters for the ENR method.

## Section 4

To assess the diagnostic ability of predictive model(s), a receiver operating characteristic curve (ROC) is often deployed (REFERENCES). The ROC curve assesses a model's predictive true positive rate (TPR) against its false positive rate (FPR) as a means to determine overall predictive strength (HANLEY). From a statistical perspective, ROC analysis can be considered as a plot of the power (probability of a test correctly rejecting the null hypothesis when an alternative hypothesis is true)

$$\begin{aligned}
TPR &= \frac{\Sigma TruePositive}{\Sigma ConditionPositive} \\
FPR &= \frac{\Sigma FalsePpositive}{\Sigma ConditionNegative} \\
FNR &= \frac{\Sigma FalseNegative}{\Sigma ConditionPositive} \\
Specificity &= \frac{\Sigma TrueNegative}{\Sigma ConditionNegative}
\end{aligned} \tag{A.16}$$

When dealing with a binary classification, as per this study, the predictive test measure for each instance is denoted by a continuous random variable (x). Given a desired threshold (T), each instance is positive if  $x > T$  and negative if  $x < T$ . Setting the probability distribution functions of the positive and negative values of x to  $f_p(x)$  and  $f_n(x)$  respectively, the . Given this, TPR is calculated as:

$$TPR(T) = \int_T^{\infty} f_p(x) dx \tag{A.17}$$

and the FNR as:

$$FPR(T) = 1 - \int_T^{\infty} f_n(x) dx \tag{A.18}$$

The ROC curve is generated by plotting  $TPR(T)$  against  $FPR(T)$  parametrically, varying across T, or as a plot of:

$$ROC(T) = 1 - f_p(f_n^{-1}(1 - T)) \quad (A.19)$$

over  $T$  from  $[0,1]$  where  $f_p^{-1}(1-T) = \inf$

Comparing the resultant ROC curves across multiple models provides the selection of the desired model based off of varying predictive accuracies. To quantify the predictive accuracy, the area under the curve (AUC) of the ROC curve is calculated, as it equals the probability of a classifier ranking a positive instance higher than a negative instance (both chosen at random).

$$\begin{aligned} A &= \int_{-\infty}^{\infty} TPR(T)FPR'(T)dT \\ &= \int_{-\infty}^{\infty} \int_{-\infty}^{\infty} I(T' > T)f_1(T')f_0(T)dT'dT = P(X_1 > X_0) \end{aligned} \quad (A.20)$$

The initial integral has reversed boundaries due to larger  $T$  values having a lower value on the x-axis.

## Section 5

Docendi eligendi sit et, pri ea dicam eligendi percipitur, has soleat dolores convenire te. Sed altera placerat an, id verterem abhorreant interesset mea. Eum at ceteros



efficiantur. Eos id voluptaria efficiendi comprehensam.

In mel modo dicam vocibus, eruditi consecutuer vim no, cu quaestio instructior eum.

Justo nostrud fuisset ea mea, eam an libris repudiandae vituperatoribus. Est choro  
corrumpit definitionem at. Vel sint adhuc vocibus ea, illud epicuri eos no. Sea simul  
officiis ea, et qui veri invidunt appellantur. Vix et eros ancillae pertinax.



# Appendix B

## Sample Code

The method for vortex identification for this study is a modification from previous work[159]. The calculation of vortex cores was based on in-house C++/Python codes derived from the open-source Vascular Modelling ToolKit (VMTK) [5]. Prior to any calculations, velocity data is first re-sampled onto a rectilinear grid whose voxel size is 0.2mm.

In the first step, the classic  $\lambda_2$  method by Jeong and Hussain [88] was used to define the negative  $\lambda_2$  region (*i.e*  $\lambda_2 < 0$ ). Then, in the second step, vortex core lines were estimated by the method proposed by Sujudi and Haines [158]. In essence, in the negative  $\lambda_2$  region, a local velocity vector  $\bar{v}$  lies along a vortex core line if the following two conditions hold: (1) the  $3 \times 3$  spatial gradient matrix of  $\bar{v}$  has two complex eigenvalues and one real eigenvalue and (2) the  $3 \times 3$  spatial gradient matrix of  $\bar{v}$  has

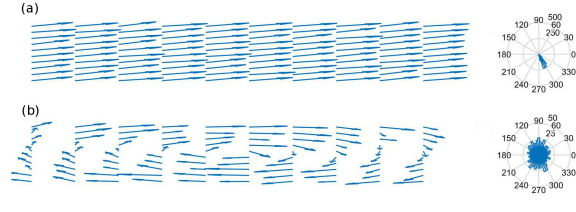


**Figure B.1:** Two examples illustrating the relationship between the angular histogram and NE: (a) a simple laminar flow case and (b) a rotational flow (eddy) case. In both cases, the right and left plots are the vector flow field and the histogram of angular vector direction, respectively. Vector fields were decimated by a factor of 3 for better visualization.

an eigenvector  $\vec{\alpha}$  corresponding to the above-mentioned real eigenvalue. Now, if we define a new scalar value  $K$  as follows,

$$K(x, y, z) = \begin{cases} |\dot{dot}(\bar{v}, \vec{\alpha})|, & \text{if } \lambda_2 < 0 \\ 0, & \text{Otherwise} \end{cases} \quad (\text{B.1})$$

where  $|\cdot|$  is an absolute operator. Of note, in Eqn. 2, both the  $\bar{v}$  and  $\vec{\alpha}$  are normalized and therefore, the scalar field  $K$  defined above is bounded between 0 and 1. If the  $K(x, y, z)$  is close to 1 then the location  $(x, y, z)$  is within the proximity of the vortex core line as suggested by Sujudi and Haimes [158].

In the third step, we calculated local normalized entropy (NE) of velocity directions [149] following work in the flow visualization literature (e.g. [118, 187]). The  $NE$  is close to 0 if the velocity direction closely concentrates one value out of  $N$  possible values (see Fig. B.1(a);  $NE=0.05$ ). In contrast, the entropy measure  $NE$  becomes

0.95 if the probability of velocity directions is almost equally likely, as shown in Fig B.1(b). Given an arbitrary voxel located at  $(x,y,z)$  within the dome of an IA, we selected a fixed volume of interest (VOI;  $N_x \times N_y \times N_z$ ;  $N_x = N_y = N_z = 11$  in this study) centered at the voxel. One additional metric  $H(x,y,z)$  can be obtained by combining  $K(x,y,z)$  together with the  $NE(x,y,z)$  as follows,

$$H(x, y, z) = K(x, y, z) * NE(x, y, z) \quad (\text{B.2})$$

$H(x,y,z)$  is a scalar field representing the likelihood of residing within a vortex core region for a location  $(x,y,z)$ .  $H$  also has a normalized range between 0 and 1. Thus, based on a fixed threshold, the vortex core region in this study can be obtained using the classic Marching-cube method [116]. in this study, 0.30 was used as the threshold for all data sets.

## HelloWorld.c

```
// HelloWorld.c
// C program to display 'Hello, World!' in the terminal.
//
// Compilation:
// gcc -g -Wall HelloWorld.c -o HelloWorld.x
//
// Execution:
```

```
// ./HelloWorld.x

// Standard headers
#include <stdio.h>

// main() begins
int main() {

    // Print the message
    printf("\n Hello, World!\n\n");

    // Indicate the termination of main()
    return 0;
}
// main() ends
```

# Appendix C

## Letters of Permission

Include letters of permission from journal editors and/or other sources from which you may have used materials (images, information, etc.) in this this work.

These materials may also be submitted separately to the Graduate School as a single, well-organized PDF file.





# Appendix D

## Cellular Biology

### TUNEL-assay

Terminal deoxynucleotidyl transferase dUTP-biotin nick end labeling (TUNEL) is an assay for detecting DNA fragmentation: an aspect of cellular damage and apoptosis. TUNEL uses the enzyme terminal deoxynucleotidyl transferase (TdT) to attach labeled deoxyuridine triphosphate (dUTP) onto the 3'-hydroxyl termini of internucleosomal DNA fragmentation. Modification of dUTP through the addition of fluorophores or haptens, such as biotin, allow for DNA fragments to be detected directly using a fluorescently-modified nucleotide and fluorescence microscopy or flow cytometry.

## VCAM-1

VCAM-1 is a member of the immunoglobulin superfamily (cell surface and soluble proteins involved in the recognition and/or binding of cells) and encodes a cell surface sialoglycoprotein (sialic acid and glycoprotein combination) expressed by cytokine-activated endothelium. This membrane protein acts as a ligand for leukocyte-endothelial cell adhesion, signal transduction, and may play a role in the development of atherosclerotic and/or inflammatory based pathologies. Molecules containing VCAM-1 counterreceptors (VLA-4 on monocytes and lymphocytes) can adhere to VCAM-1 activated cells[97]. Bound leukocytes may undergo polarized motility into the vascular wall, disrupting the cellular and matrix components of the vasculature, and degrading endothelial cell permeability.